citrOgen: a synthesis-free polysaccharide and protein antigen-presentation to antibody-induction platform

Short title: A *Citrobacter rodentium*-based antigen presentation platform

Joshua L C Wong[#,*], Julia Sanchez-Garrido[#], Jaie Rattle, Jonathan Bradshaw, Vishwas Mishra and Gad Frankel[*]

Department of Life Sciences, Imperial College London, SW7 2AZ, UK

[#]These authors contributed equally to this work

[*]For correspondence:

Electronic mail: joshua.wong@imperial.ac.uk and g.frankel@imperial.ac.uk

Keywords

Antibodies, *Citrobacter rodentium, Klebsiella pneumoniae,* type III secretion system (T3SS), EspO

Abstract

Existing technologies employed to generate antibodies against bacterial polysaccharides and proteins rely on the availability of purified or synthetic antigens. Here we present a genetics-based platform that utilises *Citrobacter rodentium* (CR), an enteric mouse pathogen, to both produce and present complex heterologous polysaccharide and protein antigens during natural infection. As a proof of concept, we use the lipopolysaccharide (O1), capsular polysaccharide (K2) and type 3 fimbrial (T3F) antigens expressed by the WHO critical priority pathogen *Klebsiella pneumoniae* (KP). Following one infection cycle (28 days) CR induces specific IgG antibodies against KPO1, KPK2 and KPT3F. We demonstrate that the antibodies are functional in downstream applications including protection against pathogenic KP challenge, KP capsular serotyping and KP biofilm inhibition. Whilst KP antigens were used as prototypical examples, this modular platform is now readily adaptable to generate antibodies against diverse polysaccharide and complex protein antigens, with basic science, public health and therapeutic applications.

36 **Introduction**

37 The specificity of antibody/antigen (Ab/Ag) binding has been widely leveraged in science,
38 biotechnology, and medicine. Both polyclonal (pAb) and monoclonal (mAb) antibodies are routinely
39 employed across these disciplines and have shaped the face of the modern practice. There is,
40 therefore, significant value in expanding the technologies available to generate new Abs that bind
41 specific Ags of interest.

42 Abs are employed widely in the field of infectious disease with both diagnostic and, more recently,
43 therapeutic applications. One key use in diagnostics is bacterial serotyping, which has played
44 important roles in pathogen epidemiology. Therapeutic Abs are licensed for both the prevention and
45 treatment of viral and bacterial infections in humans. Palivizumab, a humanised monoclonal IgG Ab
46 that binds Respiratory Syncytial Virus, was the first mAb licensed for the prophylaxis of infectious
47 disease in 1998[1]. Bezlotoxumab, a mAb against the enteric pathogen *C. difficile*, the sole mAb licensed
48 in bacterial disease, was licensed in 2016 for the secondary prevention of *C. difficile* colitis [2]. More
49 recently, during the SARS-CoV-2 pandemic, alongside vaccination, both pAb administration
50 (convalescent sera)[3] and mAbs against spike protein (e.g. bamlanivimab, etesevimab, casirivimab and
51 imdevimab)[4] were used in the prevention and treatment of COVID-19 disease. We currently have
52 limited therapeutic options to combat the antimicrobial resistance (AMR) pandemic and anti-bacterial
53 Abs (α-bAbs) are a promising modality to tackle this threat.

54 In target-specific approaches α-bAbs binding predetermined Ags are generated and selected for
55 downstream use. Target choice can be informed *a priori* by pathogen epidemiology and genomics,
56 selecting bacterial Ags that are both widespread and conserved across a bacterial species. Ags
57 representing virulence determinants can also be selectively targeted as Ab-binding has the potential
58 to functionally disrupt pathogenic mechanisms[5]. The immunisation of experimental animals or human
59 subjects is a common method to generate target-specific Abs. This results in sera containing pAb
60 secreted from reactive B-cells. These cells can be immortalised or Ab-encoding regions subcloned to

61 produce mAbs *in vitro*. Irrespective of host species, the generation of such responses is fundamentally
62 reliant on a sufficient source of conformationally correct immunogen. Generating these immunogens
63 represents a key bottleneck in target-specific Ab generation[6].

64 Polysaccharide Ags are diverse and typically composed of variable sugar subunits, each covalently
65 connected in the correct order by specific glycosidic links. These linkages can be linear or include
66 branching arrangements that determine the final polysaccharide structure. In isolation,
67 polysaccharides typically require carrier protein glycoconjugation to generate formulations that are
68 sufficiently immunogenic[6]. Production of sufficient quantities of protein Ags, which are typically affinity
69 purified following *de novo* synthesis in cells, is largely restricted to protein monomers and not
70 applicable to multiprotein complexes. The correct formation of the latter not only requires the
71 presence of chaperones and signal sequences, directing subunit assembly in the correct subcellular
72 space, but also necessitates conformationally correct monomers to interact with each other in the
73 correct stochiometric ratio. Bacterial genomes have compartmentalised the genes required to
74 synthesise both polysaccharide and multimeric protein Ags into operons, providing cloneable linear
75 DNA fragments that we exploit in the development of the technology we describe here.

76 *Citrobacter rodentium* (CR) causes colitis in mice with an infection strategy mirroring the human
77 pathogen Enteropathogenic *E. coli* (EPEC). CR attaches intimately to intestinal epithelial cells (IECs)
78 forming attaching and effacing lesions and actin-rich pedestal-like structures, a prerequisite for
79 productive infection and colitis[7]. A major virulence factor enabling CR infection is the type 3 secretion
80 system (T3SS)[8] which translocates 31 effector proteins into IECs, facilitating CR adherence and
81 proliferation [9]. The resolution of CR infection coincides with the onset of IgG secretion[10,11]. However,
82 until this adaptive immune response clears the infection, CR maintains high mucosal-associated
83 burdens, inducing significant local inflammation with associated immune cell recruitment[9]. We
84 hypothesised that this natural host-pathogen context represents an evolutionarily pre-optimised
85 environment to present alternative (heterologous) Ags to the mouse host, thereby generating mature
86 target-specific Ab responses. This hypothesis forms the basis of our platform which we term citrOgen.

87 citrOgen is a flexible and modular *in vivo* Ag presentation platform co-opting CR to present
88 heterologous Ags. It represents a single unifying genetics-based system that can be used to generate
89 functional target-specific α-bAb responses to divergent Ags in mice. We selected three structurally
90 diverse and validated Ags from the WHO critical priority pathogen *Klebsiella pneumoniae* (KP) to test
91 the platform [12]. The choice includes two surface polysaccharides, lipopolysaccharide (LPS – KP O1) and
92 capsular polysaccharide (CPS – KP K2) and a protein complex, type 3 fimbriae (KP T3F). Substituting
93 the endogenous CR O152 LPS O-Ag with KP O1 resulted in lower gut colonisation, which we overcome
94 by overexpressing the CR T3SS effector EspO. Functionally, EspO-augmented α-LPS responses potently
95 protected mice from sepsis-induced organ failure following KP challenge. We then successfully
96 generated α-CPS Abs, which we employed to serotype a diverse KP collection of 100 clinical isolates.
97 Finally, we demonstrate the platforms' ability to raise Abs to a large cell surface filamentous structure,
98 KP T3F, the regulated expression of which we designed to coincide with CR attachment to host
99 epithelia. These α-KP T3F Abs effectively blocked T3F-mediated KP biofilm formation. Together these
100 results demonstrate the ability of the platform to rapidly generate functional target-specific antibodies
101 against a broad range of major bacterial Ags.

102

103 **Results**

104 **Heterologous KP O1 O-antigen expression causes an in vivo colonisation defect**

105 Our goal was to express diverse heterologous Ags in CR to generate target-specific Abs in mice. As
106 model Ags we chose O1, K2 and T3F, the natural surface Ag configuration encoded by our prototype
107 KP strain ICC8001 (herein KP_{WT}). The *rfb* locus typically encodes all the genes required for O-Ag
108 synthesis and export in Gram-negative bacteria[13]. An exception is the KP O1 Ag, where *rfb*-derived O2
109 Ag is modified by the glycosyltransferase activity of two enzymes, WbbY and WbbZ, which are encoded
110 at a distinct chromosomal position[14]. Moreover, KP employs an ABC-transporter instead of the more
111 common *wzy*-dependent O-Ag export process used by CR_{WT}[15].

112 We started by identifying the *rfb* locus in CR_{WT}, which is encoded on the reverse strand and flanked by
113 *galF* (5') and *gnd* (3') genes (Fig 1A). We used *in silico* serotyping to confirm that CR_{WT} encodes an *E.*
114 *coli*-like O152 Ag[16]. The endogenous O152 genes were replaced with those comprising the KP O2 *rfb*
115 locus (cloned en bloc) by homologous recombination and the *wbbYZ* gene cluster inserted into the CR
116 genome by Tn7 transposon mutagenesis (Fig 1A)[17]. This strain, CR_{KPO1}, contains all the genetic
117 determinants required to synthesise and export KP O1 Ag, albeit using a non-native ABC-transporter
118 export pathway. We did not modify the CR gene products that synthesise lipid A or core oligosaccharide
119 (Fig 1B) and, therefore, CR_{KPO1} is predicted to produce a hybrid LPS molecule; the endogenous CR Raetz
120 pathway and CR *rfa* locus producing lipid A and core regions, respectively, with KP O1 Ag attached to
121 the native CR lipooligosaccharide scaffold (Fig 1B). We purified LPS from KP_{WT}, CR_{WT} and CR_{KPO1} to
122 confirm O-antigen replacement by Western blot. As anticipated α-O152 pAb sera recognised CR_{WT} but
123 was not reactive against KP_{WT} and CR_{KPO1} (Fig 1C). We then used an α-KP O1 mAb (C13)[18], which bound
124 to both KP_{WT} and CR_{KPO1}, confirming heterologous O-antigen expression in CR. The homologous
125 recombination vector employed to substitute the KP O2 locus was designed to include the endogenous
126 5' CR promoter, ensuring that future O-antigen locus substitutions can be achieved by using the same
127 vector, simply modified with O-antigen genes of choice.

128 We tested if replacing CR O152 with KP O1 affected infectivity *in vitro* and confirmed that CR_{KPO1}, like
129 $CR_{WT,}$ induced actin-rich pedestal formation following the infection of mouse fibroblasts cells.
130 Furthermore, detectable KP O1 Ag expression was restricted to CR_{KPO1} (Supplementary Fig 1A). We
131 therefore proceeded to infect CD-1 mice with 10^9 colony forming units (CFUs) of CR_{WT} or CR_{KPO1} by oral
132 gavage (Fig 1D). At 8 days post infection (dpi), when stool CR shedding peaks, faecal CR_{KPO1} CFU counts
133 were significantly lower than CR_{WT} (Fig 1D). Staining of colonic sections revealed that whilst CR_{KPO1}
134 maintained heterologous KP O1 expression *in vivo,* there were substantially fewer adhered bacteria
135 compared to CR_{WT} (Fig. 1E, Supplementary Figure 1B). These data indicated an *in vivo* colonisation
136 defect imposed by heterologous Ag expression that needed to be addressed to develop an optimal
137 platform.

138 **EspO overexpression restores CR_{KPO1} colonisation**

139 A mutant in the *Shigella flexneri* T3SS effector *ospE*, a homologue of the CR effector *espO*, results in a
140 colonisation defect in a guinea pig gut infection model, as OspE suppresses epithelial detachment[19].
141 We therefore hypothesised that over expression of EspO would promote greater bacterial attachment
142 to IECs during infection. Indeed, while deletion of *espO* in CR_{WT} showed a tendency towards decreased
143 proportion of CR-associated IECs, overexpression of EspO increased the proportion from 14.6% to
144 22.9% (Supplementary Fig 2A-C). We then overexpressed EspO in CR_{KPO1} (CR_{KPO1}+p*espO*) and infected
145 CD-1 mice; infections with CR_{WT} and CR_{KPO1} were used as controls. Enumeration of faecal CFUs now
146 revealed no difference between the faecal CFUs between CR_{WT} and CR_{KPO1}+p*espO* at 8 dpi (Fig 2A).
147 Staining of colonic sections demonstrated higher levels of CR_{KPO1}+p*espO* adhesion to the epithelia
148 compared to CR_{KPO1}, which maintained heterologous KP O1 expression *in vivo* (Fig 2B). Based on these
149 results, EspO overexpression (+p*espO*) was included in all subsequent experiments to facilitate CR
150 colonisation in the context of heterologous Ag expression.

151

152 **CR_{KPO1}+p*espO* infection elicits KP O1 specific IgG antibodies**

153 We inoculated mice with CR_{KPO1}+p*espO* and CR_{WT} by oral gavage. After CR clearance (c. 28 dpi) we
154 collected blood and assessed α-KP_{WT} IgG antibody titres by enzyme-linked immunosorbent assay
155 (ELISA), using a capture plate coated with heat-killed KP_{WT}. While control CR_{WT} mice sera had negligible
156 α-KP_{WT} IgG binding, this increased significantly in sera from CR_{KPO1}+p*espO*-infected mice, indicating
157 that we have successfully raised α-KP_{WT} Abs (Fig. 2C). To confirm the specificity of the Ab response we
158 used an isogenic rough (absent O-antigen) KP mutant, $KP_{\Delta rfb}$, and assessed binding to live bacteria by
159 flow cytometry (Fig. 2D). Consistent with the ELISA data, sera from CR_{WT}-infected mice bound to
160 neither KP_{WT} nor $KP_{\Delta rfb}$. However, sera from CR_{KPO1}+p*espO*-infected mice bound specifically to KP_{WT} and
161 not $KP_{\Delta rfb}$, confirming the presence of α-KP O1 Abs (Fig 2D, Supplementary Fig 2D). We then assessed
162 the pattern of binding to KP_{WT} by immunofluorescence (IF) microscopy (Fig 2E). This confirmed the
163 same pattern of binding of CR_{KPO1}+p*espO* sera and the reference α-KP O1 Ab C13. No detectable signal
164 was observed in sera from CR_{WT}-infected mice.

165 **Anti-KPO1 IgG Abs are functionally protective against KP pulmonary challenge**

166 We next tested the functionality of the CR_{KPO1}+p*espO*-induced α-KP O1 pAbs by lung challenge with
167 KP_{WT}. Mice that had been infected and cleared CR_{KPO1}+p*espO* were intubated and administered 500
168 CFU of KP_{WT} directly into the lungs. In preliminary experiments with CD-1 mice this KP_{WT} inoculum was
169 found to result in a progressive increase in KP CFUs in the lungs and blood resulting in a severe disease
170 phenotype at 72 h post infection (hpi) (Supplementary Fig 3 A-C). Mice that had been infected by and
171 subsequently cleared CR_{WT} were also challenged as controls. We evaluated infection outcomes by
172 assessing KP_{WT} replication and protection against host organ failure employing markers of
173 haematological, lung and renal injury in line with international consensus[20,21]. At 72 hpi KP_{WT} burdens
174 in the lungs of CR_{WT}-preinfected mice reached a median of c. 10^9 CFUs (Fig 3A). In contrast,
175 CR_{KPO1}+p*espO*-preinfected mice had significantly reduced lung CFUs with KP_{WT} only detectable in the
176 lungs of 30% (5/14) of mice. KP bacteraemia was absent in all CR_{KPO1}+p*espO*-preinfected mice in
177 comparison to 69% (9/13) of CR_{WT}-preinfected control mice (Fig 3B).

178 We then assessed if the reduction of KP_{WT} burden translated into a positive effect on host physiology.
179 Only 3 mice (20%, 3/15) in the CR_{KPO1}+p*espO*-preinfected group lost more than 10% of their starting
180 weight when challenged with KP_{WT}, whereas all mice in the CR_{WT}-preinfected group lost weight after
181 KP challenge with 86% (12/14) losing more than 10% of their starting weight (Fig 3C). Total white cell
182 counts, lymphocyte counts and platelets in the blood demonstrated significantly positive
183 improvements in CR_{KPO1}+p*espO*-preinfected mice compared to CR_{WT}-preinfected animals (Fig 3D-F).
184 Specifically, the extent of sepsis-induced leucopaenia, lymphopaenia and thrombocytopaenia were
185 abrogated by the CR_{KPO1}+p*espO* preinfection, while the number of neutrophils did not change between
186 the mouse groups (Fig 3G). Moreover, the positive acute phase reactants (APR) Serum amyloid A and
187 C-reactive protein were significantly lower in CR_{KPO1}+p*espO*-preinfected mice compared CR_{WT}-
188 preinfected animals (Fig 3H&I). This beneficial modulation in APRs translated into higher levels of the
189 negatively regulated APR, albumin, in CR_{KPO1}+p*espO* preinfected mice (Fig 3J).

190 We then used three markers to assess lung injury: IL1β and myeloperoxidase (MPO) in lung
191 homogenate and surfactant protein D (SPD) levels in the serum[20]. This revealed that CR_{KPO1}+p*espO*
192 preinfection resulted in significant reductions in IL1β and SPD levels compared to CR_{WT} preinfection,
193 indicating reduced lung inflammation and improved maintenance of the alveolar capillary barrier
194 respectively (Fig 3K&L). Preinfection with CR_{KPO1}+p*espO* also resulted in significantly reduced
195 neutrophilic alveolitis, evidenced by reduced lung MPO levels compared to CR_{WT}-preinfected mice (Fig
196 3M). Finally, we assessed acute kidney injury by measuring serum creatinine and cystatin C levels.
197 While high levels of creatinine and cystatin C were found in KP_{WT} challenged CR_{WT}-preinfected mice,
198 improvements in both excretory renal function markers were seen in CR_{KPO1}+p*espO*-preinfected mice
199 (Fig 3N&O). These data indicate that α-KP O1 Abs raised by citrOgen were protective against KP
200 challenge, restricting both bacterial replication and dissemination, and preventing KP sepsis-induced
201 organ failure.

202

203 **citroGen presentation of heterologous KP capsular polysaccharide antigen**

204 We next explore expanding the citrOgen platform to generate α-CPS Abs. KP_{WT} produces K2 CPS,
205 encoded by a c. 22Kb K2 *cps* locus, lying immediately upstream of the *rfb* locus in the KP_{WT} genome.
206 As upstream of the CR O152 *rfb* locus lie the genes involved in synthesis and export of the extracellular
207 polysaccharide colanic acid (Fig. 4A), we replaced the CR_{WT} genes between *ROD21991* and *galF* (c.
208 24kb) with the KP KL2 operon from *wzi* to *manB* by homologous recombination, generating strain
209 CR_{KPK2}+p*espO* (Fig. 4A). We chose this insertion site as we anticipate that it will tolerate other *cps* locus
210 insertions in future applications of this technology. This established vector can be used as the template
211 together with *cps* locus of choice (e.g. KP *cps* loci vary from 10-30kb and include internal promoters[22]).
212 We infected mouse fibroblasts to evaluate if the expression K2 capsule impacted on CR T3SS
213 functionality. CR_{KPK2} formed actin-rich pedestals and heterologous K2 expression was confirmed by
214 staining with reference K2 antiserum (Supplementary Fig 4A). We then infected CD-1 mice by oral
215 gavage with CR_{KPK2}+p*espO,* or CR_{WT} as a control, which were shed at comparable levels (Fig 4B).
216 Following CR_{KPK2}+p*espO* and CR_{WT} clearance, we collected blood samples and α-KP IgG levels were
217 assessed by ELISA, using KP_{WT} and an acapsular *wcaJ* mutant, $KP_{\Delta wcaJ}$. No binding to either KP_{WT} or
218 $KP_{\Delta wcaJ}$ was observed with sera from CR_{WT}-infected mice. In contrast, sera from mice infected with
219 CR_{KPK2}+p*espO* bound to KP_{WT} but not to $KP_{\Delta wcaJ}$ (Fig 4C). This indicated that KP K2 was successfully
220 presented by the citrOgen platform *in vivo* and that α-KP IgG was specifically raised against the
221 heterologous KP K2 antigen.

222 KP strains demonstrate broad diversity in CPS Ags with over 147 described to date in circulating
223 strains[22]. However, despite their key role in virulence and frequent use in genome-based epidemiology,
224 no reference antisera are currently being produced for *in vitro* applications. We used sera derived from
225 CR_{KPK2}+p*espO* infection, together with a reference K2 antiserum as a control, to stain KP_{WT}. No
226 detectable binding was seen in sera from CR_{WT}-infected mice. In contrast, binding was seen when KP_{WT}
227 was stained with the CR_{KPK2}+p*espO* sera, which phenocopied the pattern of binding seen with the

228 reference K2 antiserum (Fig. 4D). Together with the ELISA results, this provides strong evidence for
229 specific heterologous α-KP K2 Abs induced by CR_{KPK2}+p*espO* infection.

230 **KP serotyping using the citrOgen KP K2 sera**

231 We next tested if the citrOgen KP K2 sera could be used for serotyping. To this end, we used a publicly
232 available collection of 100 KP isolates, representing 54 distinct CPS types determined by genomic
233 analysis[23]. We incubated the strains with citrOgen KP K2 sera and analysed binding by flow cytometry
234 (Fig 4E, Supplementary Fig. 5B). We included KP_{WT} and $KP_{\Delta wcaJ}$ as controls and measured the median
235 fluorescence intensity (MFI) across the collection. The citrOgen KP K2 sera specifically bound KL2
236 isolates and KP_{WT} with minimal cross reactivity and absent binding to $KP_{\Delta wcaJ}$. To confirm the KL
237 assignments, we selected 9 isolates for IF with the reference K2 antisera (Fig 4F). We observed a
238 pattern of binding consistent with capsule in the KL2 strain but not the surrounding non-KL2 strains.
239 We concluded that the citrOgen KP K2 sera can be used for serotyping and validated the collection's
240 KL2 assignments.

241 **citroGen presentation of heterologous protein complex antigens**

242 We next assessed the utility of citrOgen in generating Abs against heterologous proteins, using the
243 well-conserved KP T3F as a model protein complex[24]. T3F are a KP virulence factor that mediate binding
244 to abiotic surfaces (such as plastic and glass) and are involved in the first steps of biofilm formation.
245 The major T3F subunit is MrkA which together with MrkD (adhesin tip) and MrkF (unknown function)
246 are externalised via a β-barrel transmembrane usher protein, MrkC, and assemble into T3F on the KP
247 cell surface (reviewed in Murphy et al. 2012[25]). In the periplasm a chaperone, MrkB, binds MrkA to
248 prevent ectopic pilin polymerisation. Therefore, MrkABCDF, are all required for T3F biogenesis. T3F
249 expression is tightly regulated in KP by an adjacent operon (*mrkHIJ*) via the second messenger cyclic-
250 di GMP[26]. To coordinate expression of the T3F with CR attachment to IECs *in vivo,* we constructed a
251 citrOgen strain in which *mrkABCDF* (excluding *mrkHIJ*) was driven by the promoter of the T3SS effector
252 *map* (CR_{T3F})[27]. The recombinant operon was inserted into the CR *glmS* site (Fig 5A). We perceived two
253 significant advantages of this strategy, firstly, maximising T3F expression during intimate attachment

254 to host cells and secondly to limit the metabolic burden of T3F expression in CR. To confirm accurate
255 gene regulation, we quantified *mrkA* transcript levels in T3SS-suppressing (LB media, static growth)
256 and T3SS-inducing (DMEM, static growth) conditions (Supplementary Fig 5A)[28]. qRT-PCR analysis
257 demonstrated low *mrkA* transcripts from CR_{T3F}+*pespO* grown in LB which increased significantly in
258 DMEM (Fig 5B), a change also observed for the endogenous *map* gene used as a positive control
259 (Supplementary Fig. 5A). No *mrkA* transcripts were detected in the CR_{WT} negative control. We then
260 confirmed that CR_{T3F} formed actin-rich pedestals *in vitro* and expressed KP T3F by staining with an α-
261 MrkA pAb (Supplementary Figure 5B). Finally, we tested if T3F conferred CR_{T3F} the ability to adhere to
262 glass under T3SS inducing conditions. This revealed a stark increase in the number of adhered CR_{T3F}
263 observed on glass coverslips compared to CR_{WT} when both were grown statically in DMEM, indicating
264 functional heterologous T3F expression (Fig 5C). Whilst this vector was designed to insert and provide
265 stringent control of T3F expression it can be readily be used for the expression of other operons
266 encoding mono/multimeric protein Ags to facilitate future iterations of this technology.

267 We next used oral gavage to infect CD-1 mice with CR_{T3F}+p*espO*, which colonised similarly to CR_{WT} at 8
268 dpi (Fig 5D). We used the sera collected from mice who had cleared the infection for ELISA, with plates
269 coated with heat killed KP_{WT} and $KP_{\Delta mrkA\text{-}F}$, a deletion mutant in the T3F structural genes. Sera collected
270 from the control CR_{WT}-infected mice were not reactive against KP_{WT} or the isogenic mutant (Fig 5E).
271 Conversely, sera from CR_{T3F}+*pespO* -infected mice bound $KP_{WT,}$ with absent binding to $KP_{\Delta mrkA\text{-}F.}$ This
272 data confirmed the α-KP IgG antibodies were directed towards T3F. Using pooled sera from the
273 CR_{T3F}+*pespO* infected mice to stain KP_{WT} revealed a binding pattern that matched that of the reference
274 α-MrkA pAb (Fig 5F). As T3F mediate attachment to abiotic surfaces and biofilm formation, we then
275 tested if the sera from could prevent KP_{WT} attachment. We first pre-adsorbed the sera from
276 CR_{T3F}+p*espO*- and CR_{WT}-infected mice against PFA-fixed CR_{WT} to remove α-CR Abs (10x 24h adsorption
277 cycles against fresh PFA-fixed CR_{WT}) (Supplementary Fig. 5C). This resulted in sera that negligibly bound
278 CR_{WT} (Supplementary Fig. 5D&E). We preincubated these two preadsorbed sera, which had equivalent
279 concentrations of total IgG (Supplementary Fig 5F), with KP_{WT} expressing sfGFP and measured

280 attachment after static growth at 37°C. Sera from CR_{T3F}+p*espO*-infected mice resulted in 3-fold
281 reduction in KP attachment compared to sera from CR_{WT}-infected mice (Fig. 5G &H). These data
282 demonstrate the generation of α-KP T3F Abs that functionally inhibit surface attachment, the first step
283 in KP biofilm formation.

284 **Discussion**

285 LPS, CPS and proteins are common bacterial targets where generating specific Abs is desirable. Whilst
286 techniques already exist to generate such target-specific Abs, individually tailored and time-consuming
287 approaches are required to prepare the Ags. Here, instead, we co-opt the mouse pathogen CR for this
288 purpose and combine the steps of Ag preparation and immunisation into a single platform that both
289 expresses heterologous Ags and presents them continuously, in their native conformation, to the host
290 over the entire infection cycle (Figure 6). This was achieved by recombination-based genome editing
291 in which whole operons were cloned from KP and inserted or substituted into the CR; thus, all
292 genetically encoded components are inherently included, ensuring that Ag assembly takes place in a
293 fashion mirroring the pathogen of choice. It should be noted that, whilst we achieve this for three
294 diverse Ags, they all come from KP, another Gram-negative organism, which will have favoured our
295 approach. Nevertheless, we were able to achieve specific and functional Ab responses for LPS, CPS and
296 a large protein complex. If we consider the latest iteration of the WHO Bacterial Priority Pathogens
297 List[12] then three out of four critical pathogens are Gram-negatives, indicating the clear and present
298 danger posed by this group of bacterial threats. The data we present already supports using citrOgen
299 for these organisms. We anticipate that further modifications will be required to synthesise and
300 present Gram-positive bacterial Ags. As well as the ability to present complex polysaccharide
301 structures and multicomponent protein Ags in their native location and configuration, one key
302 advantage of citrOgen is time (Fig 6). In this work we have already validated substitution/insertion sites
303 and generated the appropriate genome editing vectors. Changing the inserts encoded by these vectors
304 (to alternative LPS, CPS and protein Ags) is routine and together with subsequent CR genome editing
305 can be achieved over a period of days. Whilst we cloned sequences directly from KP DNA we propose
306 that this technology could also be applied to generate diagnostic or therapeutic Abs in an outbreak
307 scenario. The now routine use of *de novo* gene synthesis would enable us to engineer strains based on
308 early sequencing data alone. This would allow us to use this platform to generate pAb sera in as little
309 as 28 days- a complete CR infection cycle in mice. In more controlled settings we envisage generating

310 citrOgen strains encoding multiple Ags simultaneously. Ethically, this reduces the number of
311 experimental animals for use in research and development and would permit multiple target-specific
312 Ab responses to be obtained following a single infection.
313 We overcame two major obstacles to develop a viable platform for broader applicability. The first was
314 the potential fitness cost imposed by heterologous Ag expression. Indeed, we observed lower gut
315 colonisation in CR_{KPO1} than CR_{WT}, a defect that only becomes evident under the pressure of the host-
316 pathogen-microbiome environment. We overcame this obstacle by overexpressing the T3SS effector
317 EspO, which promotes IEC attachment and mucosal colonisation. The second was the metabolic cost
318 to CR of dysregulated heterologous protein expression which we overcame by placing expression
319 under the control of the endogenous CR promoter for the *map* gene. This restricts heterologous
320 protein expression to T3SS-inducing conditions and promotes presentation at host mucosal surfaces.
321 In the case of KP O1 Ag we combined citrOgen with subsequent KP lung challenge, which allowed us
322 to quantitively evaluate protection from organ failure conferred by the α-bAb response to this Ag (Fig
323 6). Given the current lack of correlates of protection for bacterial infections we propose that citrOgen
324 strains may represent an efficient tool to evaluate future proposed Ags. Strains engineered to express
325 heterologous Ags (singly or in combination) can be used to evaluate Ab responses following a CR
326 infection cycle. In the same cohort of mice, subsequent pathogenic challenge can then evaluate the
327 protection conferred by the response. Expanding the translational applicability of current priority
328 bacterial infection models would significantly enhance the data we could achieve in this approach.
329 CR infections are host restricted to mice, conferring platform safety and preventing infection risk to
330 humans. This is especially important as future citrOgen strains could include additional virulence
331 factors as Ags for Ab generation. We currently use the citrOgen platform in conventional mice
332 generating murine immunoglobulins. Advances in molecular genetics have enabled the generation of
333 'humanised' Abs initially raised in non-human species and could be applied to the current iteration of
334 the platform[29]. This improves IgG tolerability and durability when administered to human patients
335 largely by reducing the immunogenicity provoked by non-human Ig regions. Furthermore, extensive

336 work in the field of mouse genetics has enabled the generation of fully human Abs in transgenic
337 animals[30]. Combining these transgenic mice with citrOgen strain infection would result in human Ig
338 induction in one CR infection cycle (Fig 6). Existing downstream workflows, such as hybridoma
339 generation or IgG loci subcloning are already well defined and employed to produce mAbs from B-cells
340 derived from these mice. Whilst our antibiotic treatment options are rapidly diminishing the
341 application of this technology may alleviate future infectious diseases deaths by generating new Ab-
342 based diagnostic tools and therapeutics.
343

Acknowledgements

We would like to thank Professor Richard Strugnell and Dr Jonathan Wilksch at the University of Melbourne for providing the reference K2 antisera and C13 monoclonal antibody for use in this work.

We would like to thank our colleagues Dr Abigail Clements, Dr Andrew Conway Morris, Professor Victor de Lorenzo, Professor Gordon Dougan and Professor Jose Penadés for their critical assessment and feedback in writing this manuscript.

We would like to thank our colleagues Dr Mei Chong and Mr Edmond Yau in the Imperial College London Enterprise team for their support in the patent application covering the technology described in this manuscript.

Conflicts of interest

None declared.

Inclusion and diversity

We support inclusive, diverse, and equitable conduct of research.

Patent

The technology underlying citrOgen has a patent pending.

Funding

This project has been supported by grants from The Royal Society (IC160080) and Medical Research Council (MR/R02671).

362 **Figure Legends**

363 **Figure 1. Heterologous KP O1 O-antigen expression causes an *in vivo* colonisation defect.**

364 **A.** The *rfb locus* in CR_{WT} encodes a O152-like *E. coli* O-antigen locus located between *galF* and *gnd*. In

365 CR_{KPO1} the CR_{WT} *rfb* locus was substituted with the genes encoding KP O2a O-antigen and *wbbYZ*

366 (converted KP O2a to KP O1v1) inserted at the 3' *glmS* site.

367 **B.** CR_{KPO1} expresses a hybrid lipopolysaccharide molecule with native CR lipid A and core

368 lipooligosaccharide linked to KP O1 Ag. The western blot is representative of 2 biological repeats.

369 **C.** Western blot confirmation of heterologous KP O1 Ag in CR_{KPO1} performed on purified LPS

370 preparations. α-O152 Ab are immunoreactive with CR_{WT} but not KP_{WT} or CR_{KPO1} whereas α-KP O1 mAb

371 (C13) is immunoreactive with both KP_{WT} and CR_{KPO1}.

372 **D.** At 8 dpi following oral gavage, faecal CFUs are significantly lower in CR_{KPO1} compared with CR_{WT} .

373 n=10 mice per group, 2 biological repeats. Central tendency: median. Mann-Whitney test, ** exact

374 p=0.0095. GoF, gram of faeces.

375 **E.** Colonic histology was taken 8 dpi and stained for CR, KP O1 Ag; DAPI staining used as a structural

376 marker. CR_{WT} confluently adhering to the luminal surface of the colon with no detectable KP O1

377 staining. Sparse staining for CR_{KPO1} is observed with detectable KP O1 staining however, where present,

378 KP O1 Ag expression detectable. Scale bar = 200 µm. Images are representative of 3 biological repeats.

379

380 **Figure 2. CR_{KPO1} overexpressing EspO maintains infectivity and induces specific anti-KP O1 Ag IgG**
381 **responses.**

382 **A.** At 8 dpi *espO* overexpression in CR_{KPO1}+p*espO* reverses the colonisation defect observed in CR_{KPO1}
383 restoring colonisation to that of the parental CR_{WT} strain. n=15 mice per group, 3 biological repeats.
384 Central tendency: median. Ordinary one-way ANOVA with Dunnett's multiple comparison. *adjusted
385 p=0.0146 ns=non-significant. GoF, gram of faeces.

386 **B.** Colonic histology was taken 8 dpi and stained for CR and KP O1 Ag; DAPI staining used as a structural
387 marker. CR_{KPO1}+p*espO* confluently adhering to the luminal surface with KP O1 Ag expression detectable
388 and co-localising to CR staining. Sparse staining is observed for CR_{KPO1} with KP O1 Ag expression. Scale
389 bar = 200 µm. Images are representative of 3 biological repeats.

390 **C.** At 30 dpi blood was taken from the tail vein of mice that cleared CR_{WT} and CR_{KPO1}+p*espO*. ELISA,
391 using heat-killed KP_{WT} (expressing KP O1 Ag), revealed α-KP_{WT} IgG in mice following infection with
392 CR_{KPO1} +p*espO* but not CR_{WT} controls. Central tendency: mean. Mann-Whitney test, **** exact
393 p<0.0001.

394 **D.** Sera from mice was tested for binding to live KP_{WT} and $KP_{\Delta rfb}$. Binding was assessed by flow
395 cytometry and expressed as the percentage of the population positive for mouse IgG (mIgG+ve). Sera
396 from CR_{WT}-infected mice demonstrated absent binding to either KP_{WT} or $KP_{\Delta rfb}$, whereas sera from
397 CR_{KPO1}+p*espO* -infected selectively bound KP_{WT} expressing KP O1 Ag. Central tendency: mean. Unpaired
398 T-test. ns=non-significant. **** p<0.0001.

399 **E.** Sera from CR_{WT} and CR_{KPO1}+p*espO* -infected mice was used to stain KP_{WT} and image by
400 immunofluorescence microscopy. An α-KP O1 Ag mAb (C13) was used as a positive control for KP O1
401 Ag staining. CR_{WT} derived sera results in no detectable staining of KP_{WT} whereas sera from CR_{KPO1}
402 +p*espO* -infected mice and the control C13 mAb phenocopy each other with membrane-associated
403 staining of KP_{WT}.

404

405 **Figure 3. Antibodies to KP O1 O-antigen protect against KP pulmonary challenge**.

406 Mice that had cleared pre-infection with CR_{WT} and CR_{KPO1}+p*espO* were challenged by intratracheal
407 infection with 500 CFU of KP_{WT}. At 72 hpi we analysed KP replication (A&B) and host-derived severity
408 indicators (C-O). n=15 mice per group (starting) over 3 biological repeats.

409 **A&B**. KP_{WT} replication and bacteraemia are significantly reduced in the lungs (A) and blood (B) of
410 CR_{KPO1}+p*espO*-preinfected mice compared to CR_{WT} controls. . Central tendency: median. Mann-
411 Whitney tests. ****exact p<0.0001 ***exact p=0.0002.

412 **C.** KP_{WT} induces significant weight loss in CR_{WT}-preinfected mice which is reversed in CR_{KPO1}+p*espO*
413 preinfection. Central tendency: mean, error: standard deviation (SD). Mann-Whitney test. ****exact
414 p<0.0001

415 **D-F.** Clinical haematological markers of disease severity are significantly improved in CR_{KPO1}+p*espO* -
416 preinfected mice compared to CR_{WT} controls. Total white cell counts (D), lymphocyte counts (E) and
417 platelets counts (F) are significantly lower in CR_{WT}-preinfected controls indicating increased diseases
418 severity. The innate responders, neutrophils (G) are unchanged between the CR_{WT} and CR_{KPO1}+p*espO*
419 preinfected groups. Central tendency: mean, error: SD. Unpaired T-tests **p<0.0065, n=non-
420 significant.

421 **H-J.** The acute phase reactants (Serum amyloid A (H), C-reactive protein (I) and Albumin (J))
422 demonstrate a reduced inflammatory state in CR_{KPO1}+p*espO* -preinfected mice compared to CR_{WT}
423 controls. Central tendency: mean, error: SD. H&J). Mann-Whitney test, I) Unpaired T-test
424 ****p<0.0001, p**=0.0002.

425 **K-M.** Acute lung injury markers (lung homogenate IL1β (K), serum surfactant B (L) and lung
426 homogenate myeloperoxidase (M)) are improved by pre-infection with CR_{KPO1}+p*espO* compared to
427 CR_{WT} preinfection. Significant reductions in lung iIL1β, improvement in the alveolar capillary barrier
428 (surfactant protein D) and neutrophilic alveolitis (myeloperoxidase) indicate α-KP O1 Abs protect
429 against lung injury. Central tendency: mean, error: SD. K&M) Mann-Whitney test, L) Unpaired T-test
430 ****p<0.0001, ***p=0.0001, *p=0.0109.

431 **N&O.** Acute kidney injury and excretory renal failure are reduced in mice preinfected with

432 CR_{KPO1}+p*espO* compared to CR_{WT}. Serum creatinine (N) and serum cystatin C (O) are reduced in KP_{WT}

433 infected mice who have cleared preinfection with CR_{KPO1}+p*espO* compared to CR_{WT}. Central tendency:

434 mean, error: SD. Unpaired T-tests ****$p<0.0001$, ***$p=0.0006$.

435

436 **Figure 4. citrOgen derived anti-KP K2 antibodies can be used for serotyping.**

437 **A**. The *cps* in KP_{WT} is c.22kb long with 15 open reading frames. This was inserted into CR_{WT} by
438 substitution of the colanic acid biosynthesis locus generating the strain CR_{KPK2}.

439 **B.** At 8 dpi faecal CR_{KPK2}+p*espO* levels are similar to CR_{WT} . Central tendency: median. n=15 mice per
440 group, 3 biological repeats. Unpaired T-test, ns=non-significant. GoF, gram of faeces.

441 **C.** At 30 dpi blood was taken from mice that cleared infection with CR_{WT} or CR_{KPK2}+p*espO*-. An ELISA
442 was conducted against heat-killed KP_{WT} (expressing KP K2) and an isogenic acapsular mutant ($KP_{\Delta wcaJ}$).
443 CR_{WT} infected mice had no detectable IgG responses to KP_{WT} or $KP_{\Delta wcaJ}$. CR_{KPK2} infected mice had IgG
444 responses specifically against $KP_{WT.}$ n=15 mice per group, 3 biological repeats. Central tendency: mean.
445 Mann Whitney test **** p<0.0001 ns=non-significant.

446 **D.** Sera from CR_{WT} and CR_{KPK2}+p*espO*-infected mice were used to stain KP_{WT} and image by
447 immunofluorescence microscopy. An α-KP K2 pAb was used as a positive control. CR_{WT} derived sera
448 results in no detectable staining of KP_{WT} whereas sera from CR_{KPK2}+p*espO*-infected mice and the α-KP
449 K2 pAb phenocopy each other with punctate membrane-associated staining of KP_{WT}.
450 **E.** Sera from CR_{KPK2}+p*espO*-infected mice were used to serotype a collection of 100 diverse KP strains
451 with serotypes assigned by genomic analysis. Each box represents one strain with the cps (KL) type
452 described. The boxes are coloured according to the strength of binding by CR_{KPK2}+p*espO*-infected mice
453 sera, which was assessed by flow cytometry. The median fluoresence intensity (MFI) key is shown in
454 the bottom right together with staining of KP_{WT} and $KP_{\Delta wcaJ}$ controls. A box, centred on a KL2 isolate is
455 shown.

456 **F.** The strains contained within the highlighted box in (E) were stained with the reference α-KP K2 pAb
457 and imaged by immunofluorescence microscopy. The KL2 strain in the centre demonstrate punctate
458 membrane staining in keeping with K2 capsule. The other strains (non-KL2) demonstrate no staining.
459 Bacterial cell membranes were counterstained with FM-4-64 for imaging.

460

461 **Figure 5. citrOgen derived anti-KP T3F antibodies block biofilm formation.**

462 **A.** To generate a strain which expresses KP T3F the structural genes *mrkABCDF* were inserted at the 3'
463 *glmS* site in CR under the control of the T3SS effector protein Map promoter. This generated the strain
464 CR_{3F}.

465 **B.** *mrkA* transcripts were assessed by qRT-PCR from bacterial cultures of CR_{T3F} under T3SS suppressing
466 (LB) and inducing (DMEM) conditions. CR_{WT} was used as a negative control. T3SS inducing conditions
467 specifically induce *mrkA* transcription in CR_{T3F}. 4 biological replicates, central tendency mean, error
468 bars SEM. Paired T-test between LB and DMEM-grown CR_{T3F}; * $p<0.5$.

469 **C.** mCherry expressing CR_{T3F} and CR_{WT} were grown in T3SS inducing conditions on glass coverslips
470 bottomed slides. Following 6 h attachment to glass was assessed and the adhered bacteria were
471 stained for MrkA. A dense lawn of CR_{T3F} is observed binding to the glass slide with MrkA detected on
472 the cell surface indicating functional surface KP T3F expression. The parental CR_{WT} strain adheres to
473 glass slides only sparsely.

474 **D.** At 8 dpi faecal CR_{T3F}+p*espO* levels are similar to CR_{WT} . Central tendency: median. n=15 mice per
475 group, 3 biological repeats. Mann-Whitney test, ns=non-significant. GoF, gram of faeces.

476 **E.** At 30 dpi blood was taken from mice that cleared infection with CR_{WT} or CR_{T3F}+p*espO*. An ELISA was
477 conducted against heat-killed KP_{WT} (expressing KP T3F) and an isogenic mutant lacking T3F expression
478 ($KP_{\Delta A\text{-}F}$). CR_{WT} infected mice had no detectable IgG responses to KP_{WT} or $KP_{\Delta mrkA\text{-}F}$. CR_{T3F} +p*espO* infected
479 mice had specific IgG responses against $KP_{WT.}$ n=15 mice per group, 3 biological repeats. Central
480 tendency: mean. Mann Whitney test, **** $p<0.0001$, ns=non-significant.

481 **F.** Sera from CR_{WT} and CR_{T3F}+p*espO*-infected mice were used to stain KP_{WT} and image by
482 immunofluorescence microscopy. An α-MrkA pAb was used as a positive control. CR_{WT} derived sera
483 results in no detectable staining of KP_{WT} whereas sera from CR_{T3F}+p*espO*-infected mice and the α-MrkA
484 pAb phenocopy each other with spiculated membrane-associated staining of KP_{WT}.

485 **G.** CR preadsorbed sera from CR_{WT} and CR_{T3F}+p*espO*-infected mice were preincubated with KP_{WT} or
486 $KP_{\Delta mrkA\text{-}F}$ expressing sfGFP. A no-antibody was used as a control. Following 6 h of growth in M9 minimal

487 media sfGFP signal was quantified on a plate reader and presented as the KP_{WT} binding normalised to

488 $KP_{\Delta mrkA\text{-}F}$ binding. The preadsorbed sera collected from CR_{T3F}+p*espO*-infected mice specifically inhibited

489 binding compared to $CR_{WT.}$ 4 biological replicates, central tendency: mean, error bars: SEM. Repeated-

490 measures One-way ANOVA corrected with Dunnett's multiple comparisons test, * $p<0.05$.

491 **H.** The biofilm formation from (G) was assessed by imaging using sfGFP fluorescence. A large reduction

492 in adhered KP_{WT} is observed when CR_{T3F} p*espO*-infected cross adsorbed sera was incubated with KP_{WT}

493 compared to CR_{WT} cross adsorbed sera.

494

495

496 **Figure 6. The citrOgen platform as a versatile, quick and cost-efficient method of Ab production**

497 **A. citrOgen strain generation**. Selected Ag sequences are incorporated into the appropriate gene
498 editing vectors designed for optimal chromosomal expression of heterologous O-Ag, capsule or
499 complex protein Ags; p*espO* is then transformed to finalise the new citrOgen strain.

500 **B. In vivo Ab production.** The CR infection cycle and immune responses are co-opted by the citrOgen
501 platform: (i) EspO-mediated boosting of CR attachment to intestinal epithelial cells, (ii) continuous
502 exposure of immune cells to the heterologous Ags, (iii) B cell affinity maturation results in Abs,
503 primarily IgG, which mediate CR clearance by 28 dpi and can be obtained as pAb sera from blood.

504 **C. Downstream applications.** Following citrOgen infection/immunisation, the functionality of Abs can
505 be assessed *in vitro* or by *in vivo* challenge studies, the pAb sera can be used for serotyping and the B
506 cells can be used for mAb production, either by using hybridoma technology to immortalise single-cell
507 cloned B-cells or by expressing heterologous Ag-specific Ab sequences in cell lines to obtain
508 recombinant mAb.

509 Ab: Antibodies; mAb: monoclonal antibodies; pAb: polyclonal antibodies; Ag: Antigen; CR: *Citrobacter*
510 *rodentium*.

511 **Materials and Methods**

512 **Bacterial culture and antibiotics**

513 Bacteria were routinely cultured in LB Broth (Miller) (84649.05000, VWR, UK). Saturated (overnight,
514 18 h) cultures took place by inoculating broth and incubation at 37°C and shaking at 200rpm.
515 Antibiotics were added to LB broth or LB broth solidified with agar (1.10283.0500, VWR, UK) at the
516 following concentrations:
517 Gentamicin 10mcg/ml (cloning) (G1272, Merck, UK)
518 Streptomycin 50mcg/ml (cloning) (S6501, Merck, UK)
519 Kanamycin 50mcg/ml (cloning) Merck, UK)
520 Nalidixic acid 50mcg/ml (selecting CR and CFU enumeration from *in vivo* sample) (N4382, Merck, UK)
521 Rifampicin 50mcg/ml (selecting KP and CFU enumeration from *in vivo* sample) (R3501, Merck, UK)

522 **Cloning**

523 High-fidelity polymerase chain reaction was conducted using Phanta Flash (2x Phanta Flash Master Mix
524 (Dye Plus), Vazyme, China). Screening and colony polymerase chain reaction was conducted using
525 Rapid Taq (2x Rapid Taq Master Mix, Vazyme, China).
526 PCR purification (Monarch PCR & DNA Cleanup Kit (5ug), NEB) and plasmid extraction were conducted
527 with kit-based methods.
528 All mutagenesis vectors were generated by PCR products ligation via Gibson Assembly (NEB, UK)
529 according to the manufacturer's guidance.

530 **Genome editing**

531 The whole genome references sequences used for CR strain ICC168 (Nalidixic acid-sensitive version of
532 ICC169) is FN543502. The whole genome reference sequence used for ICC8001 is the closely related
533 ATCC43186-derivitive KPPR1 is CP009208.1. A list of strains generated in this work can be found in
534 Supplementary Table 1.
535 Insertions at the CR 3' *glmS* site were conducted using Tn7 mutagenesis with methods published in
536 Choi et al. Nat Methods 2005 Jun;2(6):443-8[17]. Seamless, markerless genome editing at other sites was

537 conducted by homologous recombination based on the pSEVA612S system (https://seva-
538 plasmids.com/) in both CR and KP as previously published in detail[9,31]. To improve the efficiency of
539 pSEVA612S for Gibson Assembly we further modified this plasmid by reversing the sequence of the 3'
540 ISceI endonuclease digestion site generating pSEVA612S(R). This modification improves efficiency by
541 reducing homology-based empty vector recombination.
542 All mutagenesis vectors are summarised in Supplementary Table 2. These will be submitted to a
543 publicly accessible NCBI depository upon publication. In the case where more than one vector was
544 used these are listed against the respective strain. To generate CR_{KPK2} we initially cloned a construct
545 (pSEVA612S(R)_CRColanic::K2cpsΔwbbJ_ORF) without the genes wbbJ and an annotated open reading
546 frame of unknown function according to Feldman et al Proc Natl Acad Sci U S A 2019 Sep
547 10;116(37):18655-18663[32]. We subsequently inserted these genes into our final CR_{KPK2} strain
548 (pSEVA612S(R)_ΔwbbJ::Ins_wbbJ_ORF) as new data become available according to Walker et al 2020
549 mBio 2020 Sep 22;11(5):e01750-20[33] and included the native KP promoter
550 (pSEVA612S(R)_K2:col_Pvariant_Porf2).
551 Transformation of pACYC184_espO was conducted using room temperature competent cells according
552 to our previously published protocol[31].
553 **Primers sequences available from corresponding authors upon request.**
554 **Sequencing**
555 Sanger sequencing of PCR products and plasmids was conducted by Eurofins Genomics.
556 **In silico serotyping**
557 In silico serotyping of CR was conducted using SerotypeFinder 2.0
558 (https://cge.food.dtu.dk/services/SerotypeFinder/) on genome FN543502.
559 **LPS extraction and Western Blotting**
560 LPS was extracted from 3OD units of saturated overnight cultures using a modified phenol method kit
561 (iNtRON Biotechnology, Korea) according to the manufacturer's guidance with no modification.

562 Samples were mixed with 5x Laemmli buffer and 5% 2-mercaptoethanol and separated by SDS–
563 polyacrylamide gel electrophoresis (PAGE) using a 12% acrylamide gel and tris-glycine buffer system
564 and transferred to polyvinylidene difluoride membranes (#1620177, Bio-Rad Laboratories) using a
565 TransBlot semi-dry electrophoretic transfer machine (Bio-Rad). Membranes were blocked for 2 h at
566 room temperature (RT) in 10% fat-free milk PBS–0.1% Tween 20 (PBS-T) and incubated overnight at
567 4°C with 1:500 anti-O152 or 1:2000 anti-KP O1 (Supplementary Table 3) in PBS-T with 5% BSA (A3059-
568 50G, Sigma). Secondary antibodies (Supplementary Table 3) were added diluted 1:10000 in 5% fat-free
569 milk in PBST and incubated for 1 h at RT. Immunoblots were developed with Clarity Western enhanced
570 chemiluminescence (ECL, Bio-Rad Laboratories) and images were acquired on a ChemiDoc XRS+ and
571 visualised using Image Lab software (Bio-Rad Laboratories).

572 **In vitro CR_{KPO1}, $CR_{KP\ K2}$ and CR_{T3F} infections of fibroblasts**

573 Murine Swiss 3T3 fibroblasts (ATCC® CCL-92™) were maintained in DMEM containing 4500 mg l^{-1}
574 glucose (D6546, Sigma) and supplemented with 10% fetal calf serum (F9665, Sigma) and 2 mM
575 glutaMAX (#35050061, ThermoFisher Scientific) at 37°C in 5% (v/v) CO_2 and seeded on glass coverslips
576 in 24-well plates (density $2x10^5$cells/well) for immunofluorescence. Indicated strains of CR expressing
577 mCherry from a pUltra plasmid[34] were grown to saturation in LB supplemented with gentamicin at
578 37°C with 200 rpm agitation for 8 h before subculturing 1:500 for 16 h in LB or DMEM with 1000 mg
579 l^{-1} glucose (# D5546, Sigma) at 37°C, 5% (v/v) CO_2, static. Cells were infected with the static culture at
580 a multiplicity of infection (MOI) of 100, confirmed by retrospective plating. The plate was centrifuged
581 at 1000 rpm for 5 min at RT to synchronize infection and incubated for 4 h at 37°C in a 5% CO_2
582 atmosphere. The infection was stopped with three washes with sterile phosphate-buffered saline (PBS)
583 and cells were fixed in PBS with 4% (w/v) paraformaldehyde for 15 mins at RT and washed three times
584 in PBS. Cells were then permeabilized in 0.1% (v/v) of Triton X100 in PBS for 10 min, incubated in 50
585 mM NH_4Cl in PBS as a quenching agent for 10 min, washed in PBS, and blocked in 3% BSA in PBS for 1
586 h at RT before staining with one of the following primary antibodies in 1% BSA-PBS for 1 h at RT: anti-
587 KPO1 C13 (1:200), anti-mrkA (1:100) or anti-KP K2 (1:100) (Supplementary Table 3). Coverslips were

588 washed in PBS and incubated with Alexafluor488-conjugated secondary antibodies (1:200),
589 Tetramethylrhodamine (TRITC)–conjugated phalloidin (1:500) and 4',6-diamidino-2-phenylindole
590 (DAPI) (1:1000) to label the heterologously-expressed antigen, F-actin and DNA, respectively
591 (Supplementary Table 3) in 1% BSA-PBS for 1 h. Coverslips were washed in PBS and once in water
592 before being mounted using Gold Pro-Long Anti-fade medium (#P36930, ThermoFisher Scientific) and
593 left to cure overnight at RT in the dark. Immunofluorescence images were acquired using a Zeiss
594 AxioImager Z1 microscope and processed using ZEN3.1 software (ZEN lite, Zeiss).

595 **Reverse transcription quantitative PCR (RT-qPCR)**

596 The indicated strains of CR were grown to saturation overnight in LB supplemented with the
597 corresponding antibiotics. 0.5 ml of the overnight culture were washed once in PBS, incubated in
598 RNAprotect Bacteria reagent (#76506, Qiagen) for 10 mins at RT and centrifuged at 3000 xg for 5 min.
599 The bacterial pellet was digested in 100 µl TE buffer ((30 mM Tris·Cl, 1 mM EDTA, pH 8.0) with 15 mg/ml
600 Lysozyme (L6876, Sigma-Aldrich) and 20 µl Proteinase K (#19131, Qiagen) for 10 min according to
601 manufacturer's guidelines. RNA was isolated using the RNeasy minikit (Qiagen) following the
602 manufacturer's instructions, and RNA concentration and purity was determined using a Nanodrop
603 2000 spectrophotometer (ThermoFisher Scientific). 1 µg of RNA was treated with RNase-free DNase
604 (#M6101) for 1 h at 37 °C and cDNA was then synthesized using a Moloney murine leukemia virus (M-
605 reverse transcriptase (M-MLV, #M1705) with random primers (#C1181) following the manufacturer´s
606 instructions (all from Promega). To confirm the absence of undigested DNA, a reaction mixture without
607 the M-MLV reverse transcriptase was also included (NRT). qPCR was performed using the Power Up
608 SYBR Green master mix (#A25778, ThermoFisher Scientific) and the relevant primers, whose primer
609 efficiency had been evaluated previously and determined to be 95-105% (Supplementary table 4). The
610 assay was run on a Quantstudio 1 System (Applied Biosystems, ThermoFisher Scientific) and results
611 were analysed using the QuantStudio Design & Analysis Software v1.5.2 (Applied Biosystems,
612 ThermoFisher Scientific). The relative expression level of each mRNA was evaluated using the 2-
613 ΔCtmethod, where Ct is the threshold cycle and 16S rRNA is used as the control.

614 **Whole bacterial cell ELISA**

615 To prepare heat-killed KP the indicated strains were grown overnight in LB at 37°C at 200 rpm. The
616 culture was then normalised to an optical density of 1 at 600 nm in sterile PBS, heat inactivated in the
617 presence of EDTA-free protease inhibitor cocktail (#4693159001, Sigma) at 60°C for 1 h and stored at
618 4°C until use (short-term). ELISA Flat-Bottom Maxisorp Immuno 96- Well Plates (#10547781, Fisher
619 Scientific) were incubated with 100 µL/well heat-killed CR for our serum samples or with 100 µL/well
620 goat anti-mouse IgG antibody for the standards (2 µg/µL) (Supplementary Table 3) overnight at 4°C.
621 Plates were washed three times with PBS-T, blocked for 1 h at RT with 5% BSA-PBS-T, and incubated
622 overnight at 4°C with serum samples or serially diluted mouse IgG (Supplementary Table 3) as
623 standard. Plates were washed as described above and incubated with horseradish peroxidase (HRP)-
624 conjugated goat anti-mouse IgG antibody (Supplementary Table 3) for 1 h at room temperature. Plates
625 were washed and developed by the addition of 100 µL 3,3',5,5'-tetramethylbenzidine (TMB; Thermo
626 Fisher Scientific) for 5-15 mins before stopping the reaction with 2 N H_3PO_4. The absorbances at 450
627 and 540 nm were measured in a plate reader (FLUOstar Omega; BMG Labtech), and anti-KP IgG levels
628 were quantified in samples by comparison to a mouse IgG standard curve.

629 **Determination of O-antigen-binding specificity:** KP_{WT} expressing mCherry and $KP_{\Delta rfb}$ expressing sfGFP
630 were grown as saturated overnight cultures in LB supplemented with gentamicin. On the following day,
631 both strains were mixed 1:1 (v/v) after confirming the had grown to the same optical density (600nm)
632 and transferred to a V-bottom 96-well plate (Greiner Bio-one) for staining. Single strain controls were
633 also included to ensure correct gating during flow cytometry analysis. Samples were first blocked in
634 5% BSA/PBS for 1 h at RT shaking, centrifuged at 4000 rpm, 4 °C, 10 mins and then incubated overnight
635 with sera from CR_{WT} or CR_{KPO1}+pespO-infected mice diluted 1in100 (v/v) in 1% BSA/PBS. Bacterial
636 samples were centrifuged, washed twice in cold PBS and resuspended in 1% BSA/PBS containing
637 AlexaFluor647-conjugated anti-mouse IgG (1:200, Supplementary Table 3) for 1 h at RT shaking. Cells
638 were washed twice in cold PBS, fixed in 1% PFA/PBS and kept in the dark until flow cytometry analysis.

639 Samples were acquired (minimum of 100000 bacterial cells per sample) on a Cytek Amnis CellStream
640 and data was analysed using FlowJo v10.10.0 (gating strategy shown in Supplementary Fig 3A).
641 **K2 serotyping:** The KP MRSN Diversity Panel (NR-55604) was obtained through BEI Resources, NIAID,
642 NIH[23]. The 100 strains from the MRSN collection, KP_{WT} and $KP_{\Delta wcaJ}$ (positive and negative controls
643 respectively) were grown overnight in 1mL of LB in deep well 96-well plates (VWR). 100ul of each
644 overnight was transferred to a V-bottom plate and used for staining. Plates were centrifuged at 4000
645 rpm for 10 mins at 4°C, resuspended in 5% BSA/PBS and blocked for 1 h at RT shaking using a
646 microplate mixer. Bacterial samples were then centrifuged and stained overnight at 4°C shaking using
647 sera from CR_{KPK2}+pespO-infected mice diluted 1in100 (v/v) in 1% BSA/PBS. On the following day,
648 bacterial samples were washed two times in cold PBS and stained for 1 h at RT shaking with AlexaFluor-
649 488-conjugated anti-mouse IgG (1:300; Supplementary Table 3). Cells were washed twice in cold PBS,
650 fixed in 1% PFA/PBS and kept in the dark until flow cytometry analysis. Samples were acquired on a
651 Cytek Amnis CellStream (minimum of 50000 bacterial cells per sample) and data was analysed using
652 FlowJo v10.10.0.
653 **Bacterial cell immunofluorescence microscopy (adherent protocol and suspension protocol)**
654 Adherent protocol (all ICC8001 staining)
655 mCherry expressing ICC8001 was grown as a saturated overnight culture which was sub-cultured
656 (1;1000 v/v) into M9 media (M9 salts M6030, Sigma, UK) supplemented with 0.4% glucose w/v (G8270,
657 Sigma, UK). 400ul was added into each well for imaging in a coverslip slide (µ-Slide 8 Well high Glass
658 Bottom, ibidi). Slides were grown statically at 37°C for 4 h and cells were washed in phosphate-buffered
659 saline before staining. Primary staining (sera, antibodies) took place overnight at 4°C in 0.22um filtered
660 3% bovine serum albumin (A3059, Sigma, UK)/ PBS on a rocking platform. Primary antibody was
661 removed and slides were washed 3x in PBS followed by incubation with fluorescently labelled
662 secondary antibodies (Supplementary Table 3) in 3%BSA/PBS at room temperature for 1 h on a rocking
663 platform. Slides were washed 3 times before imaging.
664

665 Suspension protocol (MRSN collection, Figure 4D)

666 MRSN collection strains were grown as saturated overnight cultures. 100ul of overnight was used for
667 staining. Following centrifugation (5000g, 5 minutes) cells were washed 3 times in PBS. Primary
668 staining (K2 antisera) took place overnight at 4°C in 3%BSA/PBS in 400ul volume with agitation. Cells
669 were washed by sequential spins (5000g, 5 minutes) and resuspension in PBS (3 washes). Secondary
670 antibody (Supplementary Table 3) was added for 45mins at room temperature in a 100ul volume with
671 agitation. Cells were washed by sequential spins (5000g, 5 minutes) and resuspension in PBS (3
672 washes). Cell membranes were then labelled with FM® 4-64 Dye (T13320, ThermoFisher Scinentific,
673 UK) at a final concentration of 5ug/ml in 100ul of PBS for 10 mins at room temperature in the dark.
674 Cells were washed once and resuspended in 100ul of fresh PBS before imaging. Cell suspension was
675 imaged on an 1% agarose (in dH_20) pad according to the following protocol (https://biotium.com/tech-
676 tips/tech-tip-imaging-bacteria-using-agarose-pads/).

677 **CR_{T3F}+p*espO* glass binding assay**

678 mCherry expressing CR_{T3F}+p*espO* and CR_{WT} were grown as saturated overnight cultures and sub-
679 cultured (1:100) into DMEM low glucose (D5546, Merck, UK) into glass coverslip slides (µ-Slide 8 Well
680 high Glass Bottom, ibidi). Slides were grown statically at 37°C for 6 h and cells were washed in
681 phosphate-buffered saline before fixing in 4% paraformaldehyde/PBS (R1026, Agar Scientific, UK) for
682 20 mins at room temperature. Cells were stained for MrkA according to the adherent protocol outlined
683 above.

684 **Pre-adsorption of CR sera**

685 Serum samples from mice infected with CR_{T3F}+pespO with anti-KP antibodies above 200ng/mL were
686 pooled; sera from CR_{WT}-infected mice were also pooled separately as a control. To inactivate
687 complement, pooled serum samples were heated at 55°C for 1 h and then were pre-adsorbed onto
688 CR_{WT} expressing sfGFP to remove CR-specific antibodies, thus enriching for anti-KP antibodies. This was
689 done by serially incubating the pooled sera samples, both from CR_{WT}- and CR_{T3F}+pespO-infected mice,
690 with ~$5x10^8$ CR_{WT} for 24 h at 4°C on a rotating wheel for 10 rounds of pre-adsorption. After each 24h-

691 incubation, the serum samples with CRWT were centrifuged at 3000 xg for 5 mins to pellet the
692 bacteria, which were kept at 4°C until flow cytometry analysis; the supernatant containing the
693 antibodies was subsequently incubated with a fresh batch of ~$5x10^8$ CR_{WT} expressing sfGFP. At the end
694 of the 8 rounds, sfGFP-expressing bacterial samples from each round of pre-adsorption with sera from
695 CR_{WT}- and CR_{T3F}+*pespO*-infected mice were stained with AF555-conjugated anti-mouse IgG (1:400;
696 Supplementary Table 3) in 2% BSA-PBS for 30 mins and analysed using a Cytek Amnis CellStream.
697 Obtained data was subsequently analysed using FlowJo v10.10.0.

698 **Dot blot**

699 Bacterial cultures were grown overnight in LB (CR) or M9 supplemented with glucose (KP), normalised
700 to an OD600 of 1 and centrifuged to pellet the cells. The pellet was resuspended in 1 ml PBS and equal
701 volumes of bacteria were then spotted onto a nitrocellulose membrane (#88018, ThermoFisher
702 Scientific) and allowed to air dry. The membrane was blocked at RT for 2 h in 5% milk-PBS-T and
703 incubated overnight at 4°C with the indicated sera diluted in 5% BSA-PBS-T to a concentration of
704 2µg/ml of total IgG. The primary was washed three times in PBS-T and a secondary HRP-conjugated
705 anti-mouse antibody (Supplementary Table 3) was added in 5% milk-PBS-T, incubated for one hour at
706 RT, and washed three times. Detection was carried out using ECL substrate (Bio-Rad) and images were
707 acquired on a ChemiDoc XRS+ and visualised using Image Lab software (Bio-Rad Laboratories).

708 **Fluorescent biofilm formation assay**

709 KP_{WT} and $KP_{\Delta mrkA\text{-}F}$ expressing sfGFP were grown overnight in M9 media and diluted into fresh M9 1:500
710 (v/v) and preincubated for 30 mins with no sera or with ~50 µg/mL IgG (1:100 dilution) of the pre-
711 adsorbed sera from either CR_{WT}- and CR_{T3F}+p*espO*-preinfected mice at RT on a rotating wheel. 100 µl
712 of each sample in triplicate were transferred into wells in a black/clear-bottom 96-well tissue-culture
713 treated plate (#353219, SLS) and incubated statically at 37℃ for 6 h. Samples were then washed 5
714 times with sterile PBS and bottom optic fluorescence readings were taken at 485/520 (Ex/Em) using a
715 FLUOstar Omega plate reader. Fluorescence values were normalised to those obtained with the

716 $KP_{\Delta mrkA\text{-}F}$ strain, which does not attach, to remove any non-specific fluorescence and reduce batch-to-
717 batch variation.

718 **Animal work**

719 All animal work was conducted at Imperial College London (Association for Assessment and
720 Accreditation of Laboratory Animal Care accredited unit) under the auspices of the Animals (Scientific
721 Procedures) Act (UK) 1986 (PP7392693). The animal work was approved locally by the institutional
722 ethics committee.

723 Female CD-1 and C57BL/6 mice were purchased from Charles River, UK. Mice were purchased at 29-
724 31 g weight (5-7 weeks) (CD-1 mice) and 18-20 g weight (6-8 weeks) (C57BL/6 mice).

725 **Husbandry**

726 Animal technicians within the facility received mice and blindly separated them into groups of 5 into
727 high-efficiency particulate air (HEPA)–filtered cages with sterile bedding. Bedding was changed weekly,
728 and enrichment supplied. Mice were housed under a 12/12-h light/dark cycle with access to food and
729 water *ad libitum*. Researchers (JSG and JLCW) conducting the work in this study were not involved in
730 selection of animals into groups as this was undertaken by technical staff prior to starting experiments.
731 Animals were identified by ear notching (conducted under restraint with no anaesthesia).

732 **CR infection by oral gavage**

733 For infections, the indicated CR strains were grown overnight in 15 ml of LB (50 ml capped Falcon
734 tubes) at 37°C and 200 rpm. The next day, the tubes were centrifuged, and the pellet was resuspended
735 in 1.5 ml of sterile PBS. Mice were infected by oral gavage with 200 µl of this solution ($1x10^9$ CFU
736 confirmed by viable counts as previously described[10]). CR faecal shedding was determined by collecting
737 stool samples at the specified days post-infection (DPI), homogenising the samples in PBS and plating
738 serial dilutions onto LB agar containing nalidixic acid. Plates were incubated at 37°C overnight and
739 colonies were counted on the following day.

740

741 Mice were culled at 6 (C57BL/6) or 8 dpi (CD-1) and colons were extracted for downstream processing.
742 When characterising antibody responses, mice were followed until clearance of CR infection and then
743 culled to obtain sera or challenged with KP infection.

744 **Colonic histology processing and immunostaining**

745 At 8 dpi, the colon was extracted, and the distal 0.5 cm was fixed in 4% PFA for 2 hours and then kept
746 in 70% ethanol until processing. Fixed tissues were processed, paraffin embedded, and sectioned at 5
747 µm. For immunofluorescence, sections were dewaxed by submersion in HistoClear II solution
748 (#101412-884, VWR) twice for 10 min, 100% ethanol twice for 10 min, 95% ethanol twice for 10 min,
749 80% ethanol once for 3 min, and PBS-0.1% Tween 20-0.1% saponin (PBS-TS) twice for 3 min.
750 Subsequently, sections were heated for 30 min in demasking solution (0.3% trisodium citrate-0.05%
751 Tween 20 in distilled H2O). Once cooled, slides were first blocked in PBS-TS supplemented with 10%
752 normal donkey serum (NDS, D9663, Sigma) for a minimum of 1 h in a humid chamber, before being
753 incubated with anti-CR antibody (1:50) and anti-KP O1 (1:100) diluted in PBS-TS with 10% NDS
754 overnight at 4°C. Slides were rinsed twice for 10 min each time in PBS-TS, followed by incubation with
755 Alexafluor488-conjugated secondary antibodies (1:100) and DAPI (1:1000) (Supplementary Table 3).
756 Washing steps were repeated before slides were mounted with ProLong Gold antifade mountant.
757 Images were acquired using a Zeiss AxioVision Z1 microscope using a Hamamatsu microscope camera
758 and processed using ZEN3.1 software (ZEN lite, Carl Zeiss MicroImaging GmbH, Germany).

759 **cIEC isolation and flow cytometry analysis**

760 Colonic intestinal epithelial cells (cIECs) from mock-infected and CR-infected C57BL/6 mice were
761 isolated from 2-cm distal colonic tissue samples as previously described[35]. Briefly, the 2-cm colonic
762 tissue sample was opened longitudinally and washed in 1× Hanks' balanced salt solution (HBSS)
763 without Mg and Ca (# 14185045, ThermoFisher Scientific) and incubated at 37°C, 200 rpm for 45 min
764 in IEC dissociation buffer (1× HBSS, 10 mM HEPES, 1 mM EDTA, and 5 µL/mL 2-β-mercaptoethanol).
765 The remaining tissue was removed, and detached cells were collected by centrifugation (3000 rpm for
766 10 min), followed by two DPBS (#D8537, Sigma) washes at 4°C. Cells were then incubated 5 mins at RT

767 with 50 µg/mL DNase I (#11284932001, Sigma) to digest extracellular DNA and passed through a 70-
768 µm cell strainer on ice to ensure a single-cell suspension, pooling samples from the same group and
769 rinsing with 20 mL of cold DPBS. All steps from here onwards were performed on ice/at 4°C to maintain
770 cell viability. cIECs were counted using trypan blue to exclude dead cells and ~$1x10^7$ live cells were
771 centrifuged, resuspended in fluorescence-activated cell sorter (FACS) buffer (5% FBS, 2mM EDTA in
772 DPBS) supplemented with Fc block (#130-092-575, Miltenyi Biotec) and incubated for 10 min. Samples
773 were then incubated with FACS buffer containing anti-CR (1:1000) for 20 mins, washed twice in and
774 then incubated with EpCAM-APC (1:100) and phycoerythrin (PE) anti-rabbit IgG (Supplementary Table
775 3) for 40 min, washed, and fixed in 1% paraformaldehyde in PBS prior to analysis on a BD LSRFortessa
776 cell analyser (BD Biosciences). Data were analysed using FlowJo v10.10.0 and the gating strategy is
777 shown in Supplementary Fig. 2A.

778 **Tail vein bleeds and serum separation**

779 Small volume bleeds (<100ul) were conducted on conscious, restrained mice using a Tail Vein Injection
780 platform (Hugeiron, MouseSerum, China). Blood was taken from the lateral tail vein by puncture with
781 a 25G needle and collected via pipette into a paediatric serum collection tube (Microvette® 100 Serum
782 Cat, Starstedt). Following 1 hour of clotting at RT, sera was separated by centrifugation at 20 000g for
783 3 minute. Separated sera was stored at -80°C until use.

784 **KP pulmonary infections**

785 Anaesthesia (ketamine 80mg/kg and medetomidine 0.8mg/kg) was delivered by intraperitoneal
786 injection. Body temperature was maintained with a heat mat throughout until recovery or during the
787 intubation procedure itself.

788 Intubation was achieved with a 20G cannula (BD Insyte, BD) using the commercially supplied
789 intubation kit (Endotracheal Mouse Intubation Kit, ETI-MSE, Kent Scientific). 50ul of inoculum (diluted
790 in phosphate buffered saline) was delivered into the hub of the 20G cannula and drawn into the lungs
791 by spontaneous ventilation.

792

793 Recovery took place at 32°C in a forced air heating cabinet. At 15 minutes post anaesthesia induction
794 medetomidine was reversed by the administration of 0.8mg/kg atipamezole, delivered by
795 subcutaneous injection into the neck scruff.
796 The total volume of administered drugs was designed to deliver 20mg/kg of total fluids to animals, a
797 human paediatric resuscitation dose.
798 Mice were returned to their home individual ventilated cages after they were spontaneously moving
799 and checked at regular intervals post infection.
800 **Cardiac puncture**
801 Mice were weighed at end-point (after clearance for CR infected animals and 72 hpi for KP-challenged
802 animals).
803 Anaesthesia (ketamine 100mg/kg and medetomidine 1mg/kg) was delivered by intraperitoneal
804 injection. Mice were checked and following the absence of pedal reflexes placed in dorsal recumbency.
805 Paws were taped to a board and scissors used to remove the skin over the xiphisternum. Blood was
806 collected from the right ventricle (closed approach) with a 25G needle inserted at 30° to the skin
807 surface until blood was freely aspirated into a 1ml syringe.
808 When blood was obtained for determination of IgG titres (i.e mice infected with indicated CR strains
809 expressing heterologous antigens), the 25G needle was removed (to prevent haemolysis) and the
810 blood was transferred to a serum collection tube containing a clot activator (BD Microtainer SST with
811 separating gel, BD). Blood in the serum tube was allowed to clot for 1 hour at RT before centrifugation
812 (20 000 xg) for 3 minutes. The sera was divided into aliquots and stored at -80°C until use.
813 When blood was obtained from KP challenged mice, 20ul of whole blood was taken for CFU
814 enumeration by plating 10-fold serial dilutions (in PBS supplemented with 1mmol EDTA to prevent
815 clotting) on LB Agar plates containing rifampicin 50ug/ml. The 25G needle was again removed and
816 approximately 50-100 µl placed immediately into a tube coated with EDTA for anticoagulation
817 (Microvette® 100 EDTAK3E, 100ul, Sarstedt) for haematological analysis. The remaining blood
818 (approximately 800 µl) was allowed to clot for 1 hour at room temperature in a serum collection tube

819 as described above, before centrifugation (20 000g) for 3 minutes. The sera was divided into aliquots
820 and stored at -80°C until use.

821 **Lung homogenate processing**

822 Post-mortem lungs were removed and placed in 3ml of phosphate buffered saline in a gentleMACS C-
823 tube (Miltenyi Biotec). These were homogenised on a gentleMACS Octo Dissociator (Miltenyi Biotec)
824 using the program m_lung_2. The program was run twice in succession to achieve uniform
825 homogenisation.

826 30ul of lung homogenate was taken for CFU enumeration by plating 10-fold serial dilutions on LB Agar
827 plates containing rifampicin 50ug/ml.

828 1ml of lung homogenate was transferred into a 1.5ml microcentrifuge tube and spun at 10 000 xg for
829 5 minute at 4°C to pellet out particulate matter. The supernatant was stored -80°C for future use.

830 **HM5 analysis of EDTA anticoagulated whole blood**

831 Anticoagulated blood was run on the HM5 Vetscan analyser according to the manufacturer's
832 instruction. Outcome variables of infection were assessed using the kits summarised in Supp Table 5
833 according to the manufacturer's guidelines with the following specifications.

834 **Capture ELISAs:** ELISAs were performed using ELISA Clear Flat-Bottom Maxisorp Immuno 96- Well
835 Plates (#10547781, Fisher Scientific). Samples were added to coated and blocked plates and incubated
836 overnight at 4 degrees for all ELISAs. The range of sample dilutions used for each ELISA is indicated in
837 Supplementary Table 5; serial dilutions in the corresponding assay diluent were performed when
838 samples needed to be diluted further than 1in50. After addition of the TMB substrate solution (#00-
839 4201-56, ThermoFisher Scientific) to the wells at the end of the assay, these were incubated at RT until
840 a clear gradation in colour could be seen from the highest to the lowest standard, at which point the
841 reaction was stopped by adding 1M phosphoric acid (Sigma). All absorbance readings were obtained
842 using a using a FLUOstar Omega plate reader and readings at 540 nm were subtracted from absorbance
843 readings at 450nm to correct for optical imperfections of the plate. All ELISAs included blanks and
844 standard curves with at least 7 points within range. Sample values were obtained by interpolation into

845 the standard curve; any samples with values out of the range of the standard were assayed again at a
846 dilution(s) that ensured the value was within range.
847 **Albumin:** All reactions were done in a total volume of 200 µl in an untreated 96 well plate (Greiner
848 Bio-one) to allow vigorous shaking after reagent addition. Samples and standard were diluted 1:5 in
849 PBS (0.01 M, pH 7.4) and 5 µl were added per well; 5 µl of double-distilled water were added to the
850 blank. Subsequently 195 µl of stock working solution (prepared according to the manufacturer's
851 instructions) were added into each well, mixed thoroughly using a plate mixer and then left to stand
852 at RT for 10 mins before measuring the absorbance of each well at 628 nm using a FLUOstar Omega
853 plate reader.
854 **Creatinine:** Serum samples did not require deproteinization. The assay was performed using the
855 colorimetric reaction mix, and readings were acquired by measuring absorbance at 570 nm using a
856 FLUOstar Omega plate reader. High levels of haemolysis lead to high background due to the colour;
857 background control samples (ie sample with no creatininase) were essential in those cases. 40 µl of
858 serum sample and 10 µl of assay buffer were used per sample well; standards were prepared according
859 to the manufacturer's instructions. After interpolating into the standard curve and correcting for
860 sample dilution, the values are given as nmol/ 50 µl sample; these were transformed to mg/dL, where
861 the molecular weight of creatinine is 113.12 mg/mmol.
862 **Data analysis and visualisation**
863 Graphs and statistical analysis was carried out in GraphPad Prism version 10.4.1 for Windows and
864 version 10.4.0 for Mac (GraphPad Software, Boston, Massachusetts USA, www.graphpad.com). Data
865 were analysed for normal distribution based on D'Agostino-Pearson or Shapiro-Wilk normality tests
866 before performing any statistical analyses. Normally distributed data was analysed with the parametric
867 tests detailed in the figure legends; indicated non-parametric tests were applied to data that failed to
868 meet the normality criteria. When more than three comparisons were made, *p* values were adjusted
869 for multiple comparisons as indicated in the figure legends (Dunnett's post hoc test). For ELISAs, two
870 or three technical replicates were used to estimate experimental mean. Statistical significance was

871 only determined in datasets where each group had three or more biologically independent repeats. A

872 *p* value <0.05 is considered statistically significant.

873 Schematics in Supplementary Fig. 5C and Fig. 6 were made using some images from BioRender

874 (created with BioRender.com). Images were edited and compiled into figures in Affinity Designer V2.

875 (Serif Europe Ltd).

References

1. El-Atawi, K. *et al.* Efficacy and Safety of Palivizumab as a Prophylaxis for Respiratory Syncytial Virus (RSV) Disease: An Updated Systemic Review and Meta-Analysis. *Cureus* **15**, e51375 (2023).
2. Thandavaram, A. *et al.* The Efficacy of Bezlotoxumab in the Prevention of Recurrent Clostridium difficile: A Systematic Review. *Cureus* **14**, e27979 (2022).
3. Self, W. H. *et al.* Neutralizing COVID-19 Convalescent Plasma in Adults Hospitalized With COVID-19: A Blinded, Randomized, Placebo-Controlled Trial. *Chest* **162**, 982–994 (2022).
4. Focosi, D., Franchini, M., Casadevall, A. & Maggi, F. An update on the anti-spike monoclonal antibody pipeline for SARS-CoV-2. *Clin Microbiol Infect* **30**, 999–1006 (2024).
5. Tkaczyk, C. *et al.* Identification of anti-alpha toxin monoclonal antibodies that reduce the severity of Staphylococcus aureus dermonecrosis and exhibit a correlation between affinity and potency. *Clin Vaccine Immunol* **19**, 377–85 (2012).
6. Zhu, H., Rollier, C. S. & Pollard, A. J. Recent advances in lipopolysaccharide-based glycoconjugate vaccines. *Expert Rev Vaccines* **20**, 1515–1538 (2021).
7. Mundy, R., MacDonald, T. T., Dougan, G., Frankel, G. & Wiles, S. Citrobacter rodentium of mice and man. *Cell Microbiol* **7**, 1697–706 (2005).
8. Sanchez-Garrido, J., Ruano-Gallego, D., Choudhary, J. S. & Frankel, G. The type III secretion system effector network hypothesis. *Trends Microbiol* **30**, 524–533 (2022).
9. Ruano-Gallego, D. *et al.* Type III secretion system effectors form robust and flexible intracellular virulence networks. *Science* **371**, (2021).
10. Crepin, V. F., Collins, J. W., Habibzay, M. & Frankel, G. Citrobacter rodentium mouse model of bacterial infection. *Nat Protoc* **11**, 1851–76 (2016).
11. Dennis, A. *et al.* The p50 subunit of NF-kappaB is critical for in vivo clearance of the noninvasive enteric pathogen Citrobacter rodentium. *Infect Immun* **76**, 4978–88 (2008).
12. World Health Organization. *WHO Bacterial Priority Pathogens List, 2024: Bacterial Pathogens of Public Health Importance to Guide Research, Development and Strategies to Prevent and Control Antimicrobial Resistance.* (2024).
13. Whitfield, C. & Trent, M. S. Biosynthesis and export of bacterial lipopolysaccharides. *Annu Rev Biochem* **83**, 99–128 (2014).
14. Vinogradov, E. *et al.* Structures of lipopolysaccharides from Klebsiella pneumoniae. Eluicidation of the structure of the linkage region between core and polysaccharide O chain and identification of the residues at the non-reducing termini of the O chains. *J Biol Chem* **277**, 25070–81 (2002).
15. Bronner, D., Clarke, B. R. & Whitfield, C. Identification of an ATP-binding cassette transport system required for translocation of lipopolysaccharide O-antigen side-chains across the cytoplasmic membrane of Klebsiella pneumoniae serotype O1. *Mol Microbiol* **14**, 505–19 (1994).
16. Joensen, K. G., Tetzschner, A. M. M., Iguchi, A., Aarestrup, F. M. & Scheutz, F. Rapid and Easy In Silico Serotyping of Escherichia coli Isolates by Use of Whole-Genome Sequencing Data. *J Clin Microbiol* **53**, 2410–26 (2015).
17. Choi, K.-H. *et al.* A Tn7-based broad-range bacterial cloning and expression system. *Nat Methods* **2**, 443–8 (2005).
18. Clements, A. *et al.* Targeting subcapsular antigens for prevention of Klebsiella pneumoniae infections. *Vaccine* **26**, 5649–53 (2008).
19. Kim, M. *et al.* Bacteria hijack integrin-linked kinase to stabilize focal adhesions and block cell detachment. *Nature* **459**, 578–82 (2009).
20. Matute-Bello, G. *et al.* An official American Thoracic Society workshop report: features and measurements of experimental acute lung injury in animals. *Am J Respir Cell Mol Biol* **44**, 725–38 (2011).

927 21. Osuchowski, M. F. *et al.* Minimum quality threshold in pre-clinical sepsis studies (MQTiPSS):
928 an international expert consensus initiative for improvement of animal modeling in sepsis.
929 *Intensive Care Med Exp* **6**, 26 (2018).
930 22. Lam, M. M. C., Wick, R. R., Judd, L. M., Holt, K. E. & Wyres, K. L. Kaptive 2.0: updated capsule
931 and lipopolysaccharide locus typing for the Klebsiella pneumoniae species complex. *Microb*
932 *Genom* **8**, (2022).
933 23. Martin, M. J. *et al.* A panel of diverse Klebsiella pneumoniae clinical isolates for research and
934 development. *Microb Genom* **9**, (2023).
935 24. Old, D. C. & Adegbola, R. A. A new mannose-resistant haemagglutinin in Klebsiella. *J Appl*
936 *Bacteriol* **55**, 165–72 (1983).
937 25. Murphy, C. N. & Clegg, S. Klebsiella pneumoniae and type 3 fimbriae: nosocomial infection,
938 regulation and biofilm formation. *Future Microbiol* **7**, 991–1002 (2012).
939 26. Yang, J. *et al.* Transcriptional activation of the mrkA promoter of the Klebsiella pneumoniae
940 type 3 fimbrial operon by the c-di-GMP-dependent MrkH protein. *PLoS One* **8**, e79038 (2013).
941 27. Ma, C. *et al.* Citrobacter rodentium infection causes both mitochondrial dysfunction and
942 intestinal epithelial barrier disruption in vivo: role of mitochondrial associated protein (Map).
943 *Cell Microbiol* **8**, 1669–86 (2006).
944 28. Leverton, L. Q. & Kaper, J. B. Temporal expression of enteropathogenic Escherichia coli
945 virulence genes in an in vitro model of infection. *Infect Immun* **73**, 1034–43 (2005).
946 29. Riechmann, L., Clark, M., Waldmann, H. & Winter, G. Reshaping human antibodies for
947 therapy. *Nature* **332**, 323–7 (1988).
948 30. Lee, E.-C. *et al.* Complete humanization of the mouse immunoglobulin loci enables efficient
949 therapeutic antibody discovery. *Nat Biotechnol* **32**, 356–63 (2014).
950 31. Wong, J. L. C. *et al.* OmpK36-mediated Carbapenem resistance attenuates ST258 Klebsiella
951 pneumoniae in vivo. *Nat Commun* **10**, 3957 (2019).
952 32. Feldman, M. F. *et al.* A promising bioconjugate vaccine against hypervirulent Klebsiella
953 pneumoniae. *Proc Natl Acad Sci U S A* **116**, 18655–18663 (2019).
954 33. Walker, K. A., Treat, L. P., Sepúlveda, V. E. & Miller, V. L. The Small Protein RmpD Drives
955 Hypermucoviscosity in Klebsiella pneumoniae. *mBio* **11**, (2020).
956 34. Mavridou, D. A. I., Gonzalez, D., Clements, A. & Foster, K. R. The pUltra plasmid series: A
957 robust and flexible tool for fluorescent labeling of Enterobacteria. *Plasmid* **87–88**, 65–71
958 (2016).
959 35. Hopkins, E. G. D., Roumeliotis, T. I., Mullineaux-Sanders, C., Choudhary, J. S. & Frankel, G.
960 Intestinal Epithelial Cells and the Microbiome Undergo Swift Reprogramming at the Inception
961 of Colonic Citrobacter rodentium Infection. *mBio* **10**, (2019).
962

FIGURE 1.

A.

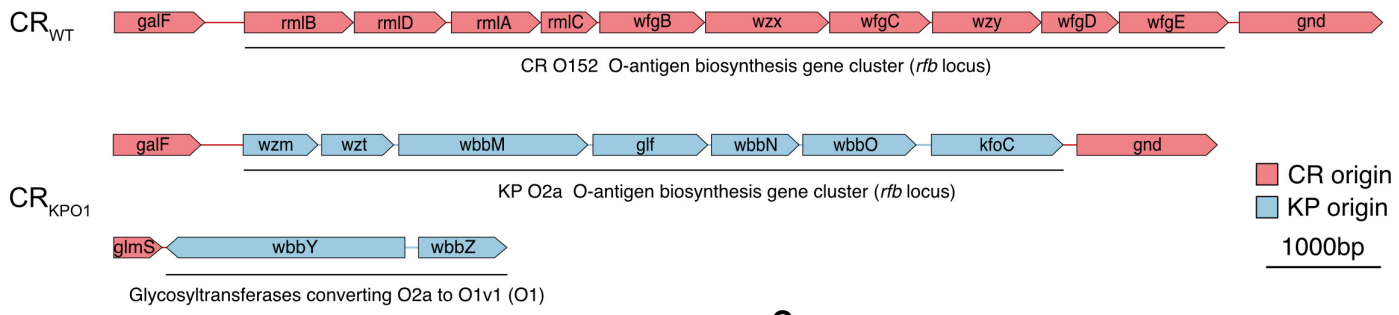

B.

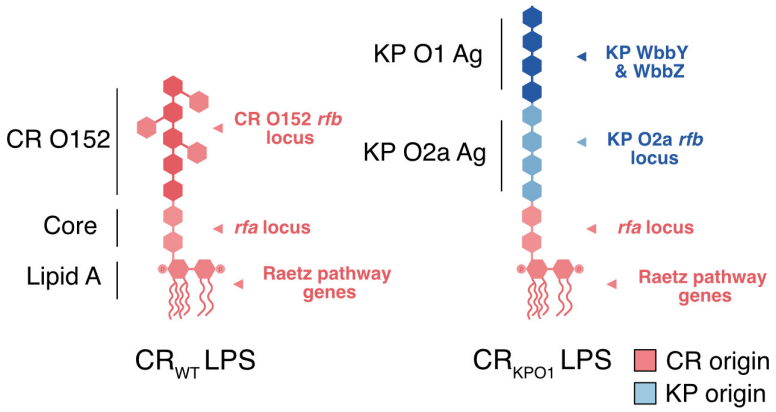

C.

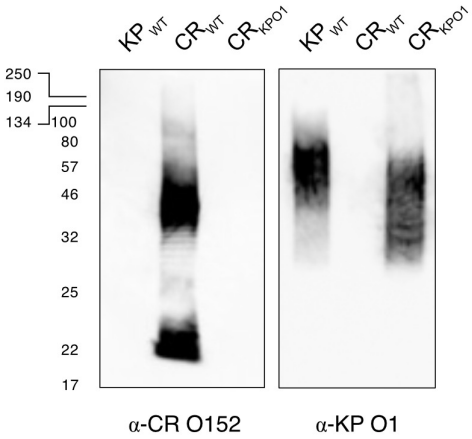

D.

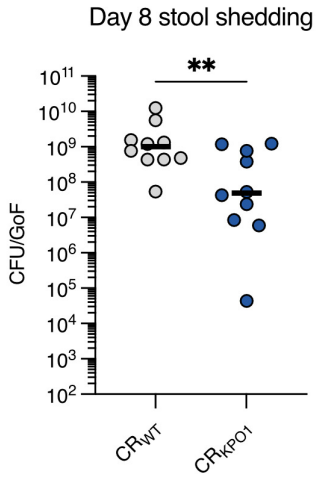

E.

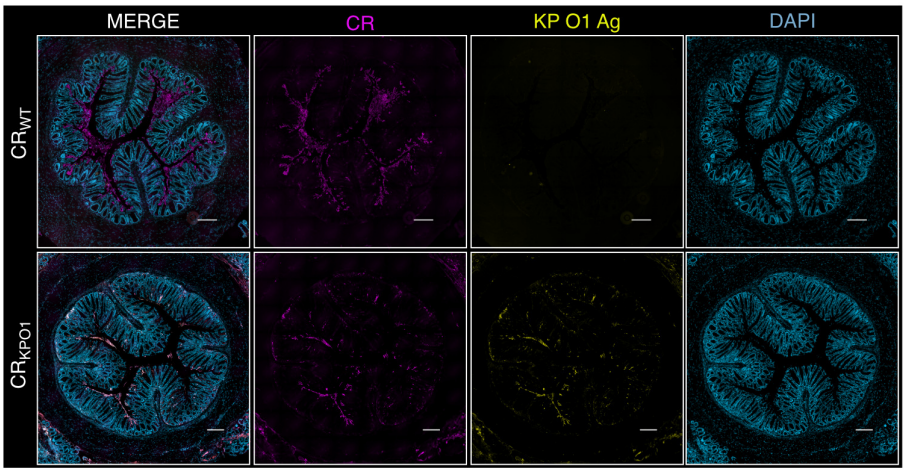

FIGURE 2.

A.

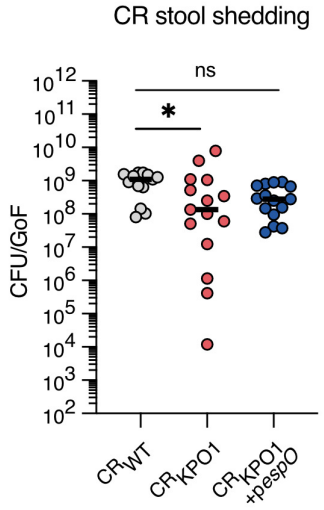

B.

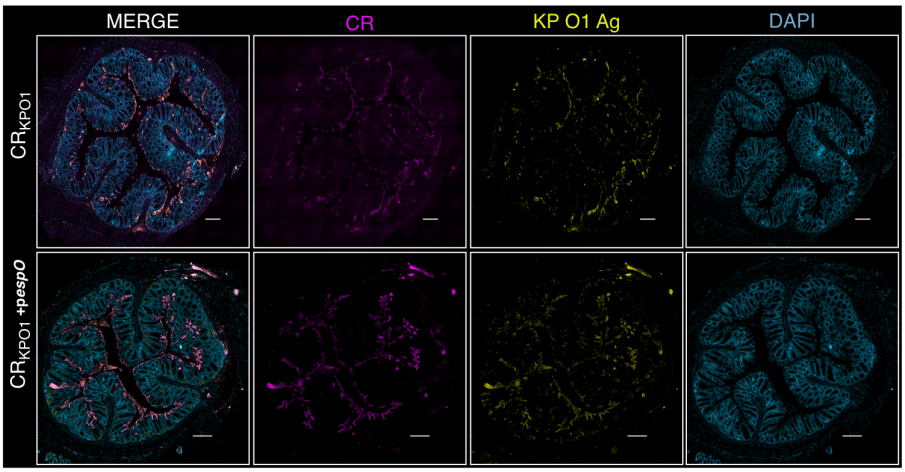

C.

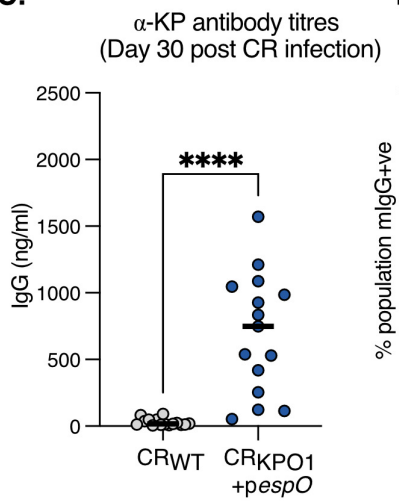

D.

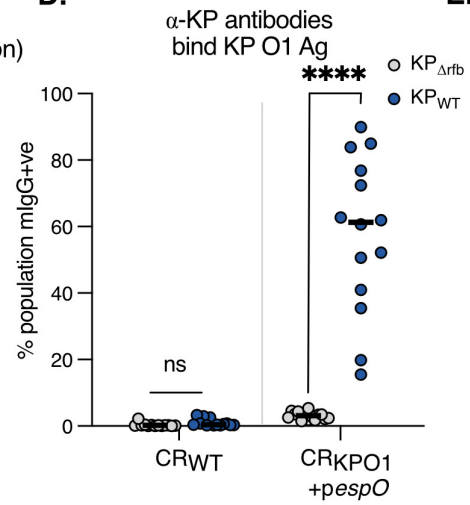

E.

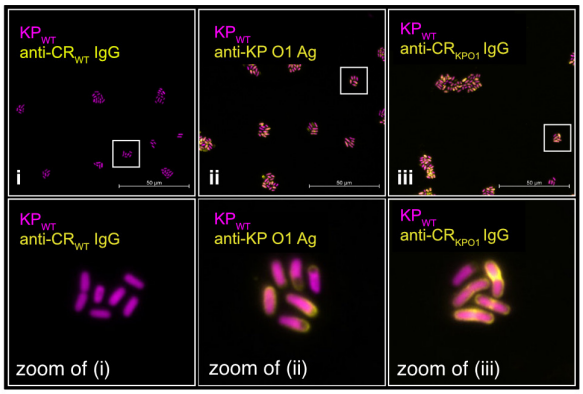

FIGURE 3.

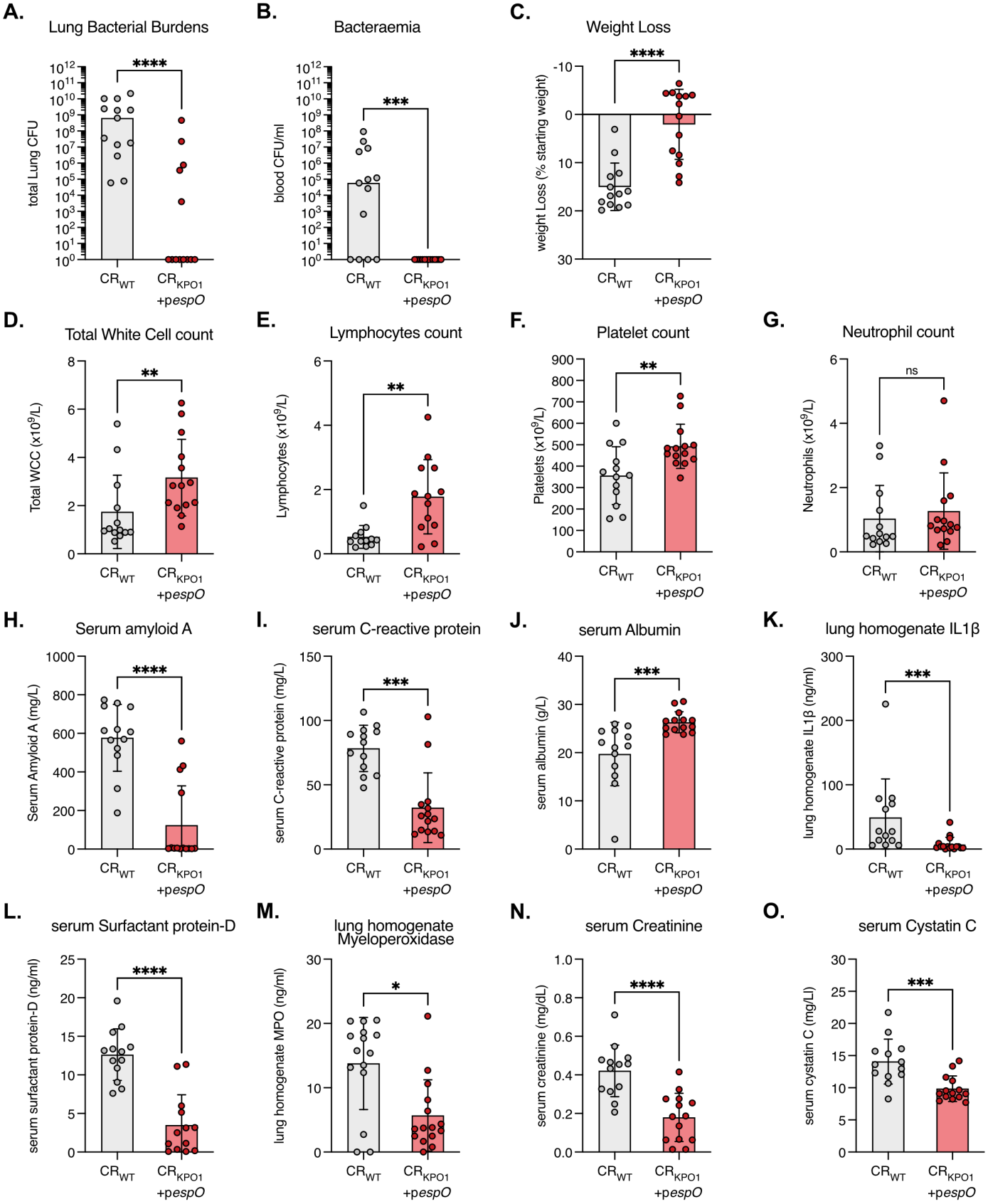
A.
Lung Bacterial Burdens
total Lung CFU
****
B.
Bacteraemia
blood CFU/ml
***
C.
Weight Loss
weight Loss (% starting weight)
****
D.
Total White Cell count
Total WCC (x10^9/L)
**
E.
Lymphocytes count
Lymphocytes (x10^9/L)
**
F.
Platelet count
Platelets (x10^9/L)
**
G.
Neutrophil count
Neutrophils (x10^9/L)
ns
H.
Serum amyloid A
Serum Amyloid A (mg/L)
****
I.
serum C-reactive protein
serum C-reactive protein (mg/L)
***
J.
serum Albumin
serum albumin (g/L)
***
K.
lung homogenate IL1β
lung homogenate IL1β (ng/ml)
***
L.
serum Surfactant protein-D
serum surfactant protein-D (ng/ml)
****
M.
lung homogenate Myeloperoxidase
lung homogenate MPO (ng/ml)
*
N.
serum Creatinine
serum creatinine (mg/dL)
****
O.
serum Cystatin C
serum cystatin C (mg/Ll)
***
CR_WT
CR_KPO1 +pespO

FIGURE 4.

A.

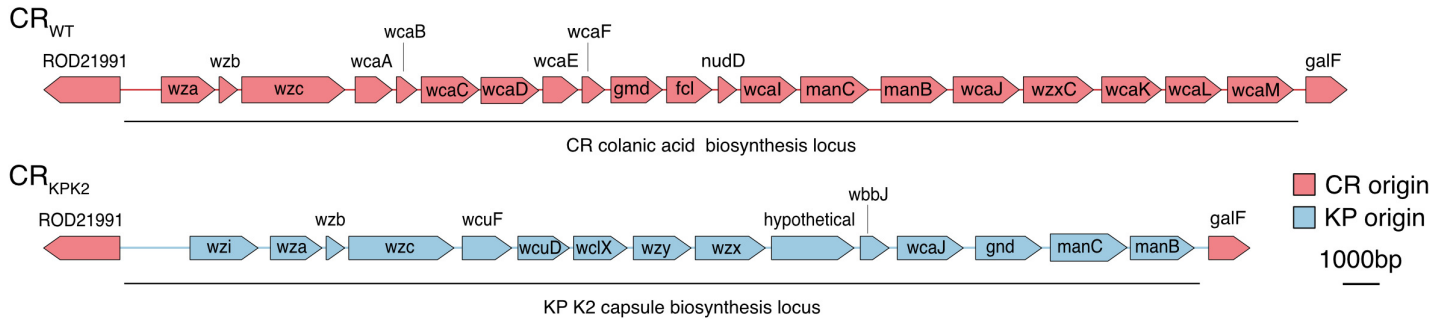

B.

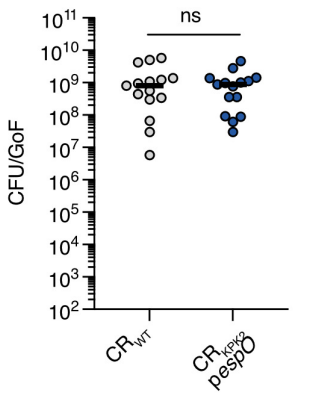

C.

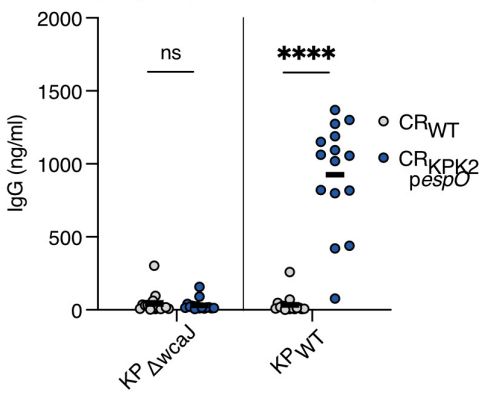

D.

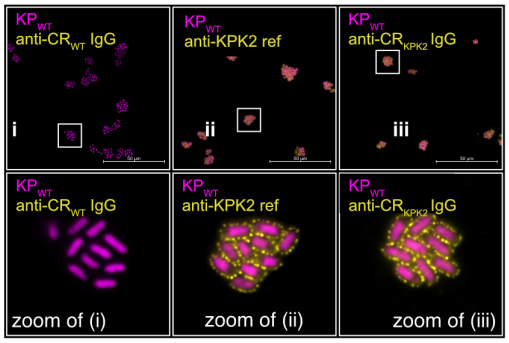

E.

KL25	KL31	KL38	KL38	KL148	KL30	KL62	KL17	KL3	KL25
KL23	KL10	KL3	KL17	KL142	KL60	KL62	KL113	KL42	KL63
KL2	KL14	KL28	KL24	KL28	KL105	KL151	KL102	KL30	KL52
KL19	KL30	KL119	KL110	KL3	KL154	KL146	KL27	KL15	KL125
KL51	KL64	KL2	KL52	KL57	KL5	KL3	KL25	KL51	KL57
KL21	KL107	KL15	KL113	KL58	KL51	KL10	KL2	KL30	KL1
KL43	KL30	KL64	KL61	KL27	KL9	KL46	KL36	KL116	KL62
KL2	KL35	KL20	KL28	KL13	KL61	KL2	KL51	KL112	KL14
KL102	KL62	KL39	KL30	KL46	KL15	KL14	KL65	KL54	KL107
KL122	KL46	KL15	KL2	KL2	KL128	KL62	KL107	KL64	KL107

KP$_{WT}$
KP$_{\Delta wcaJ}$

MFI signal key

2000
1000
500
250
125
62.5
31.3

F.

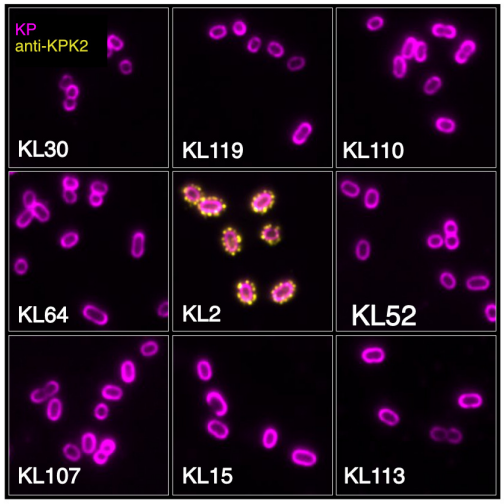

FIGURE 5.

A.

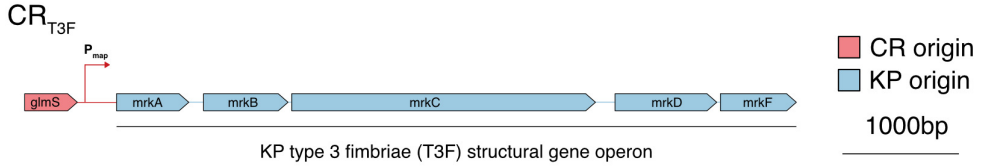

B.

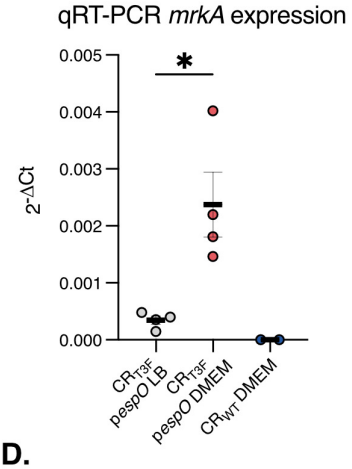

C.

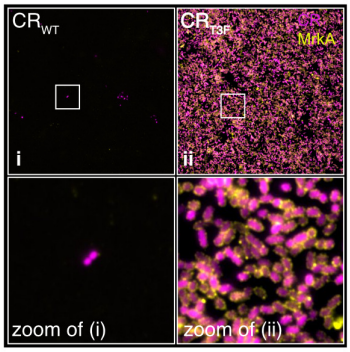

D.

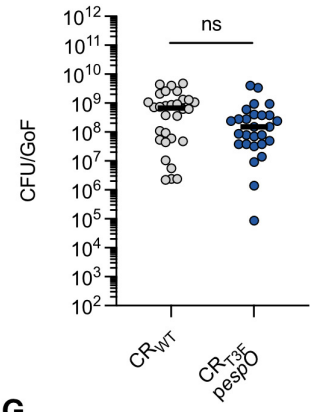

E.

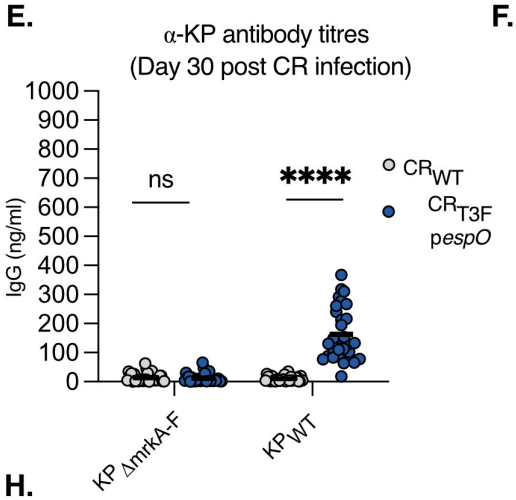

F.

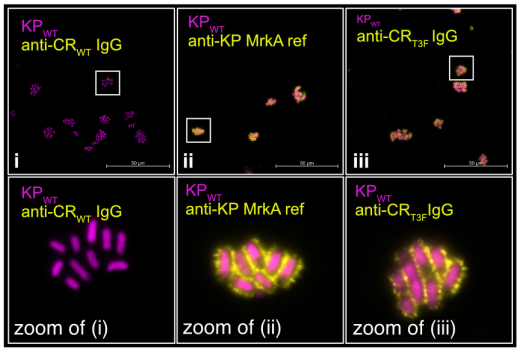

G.

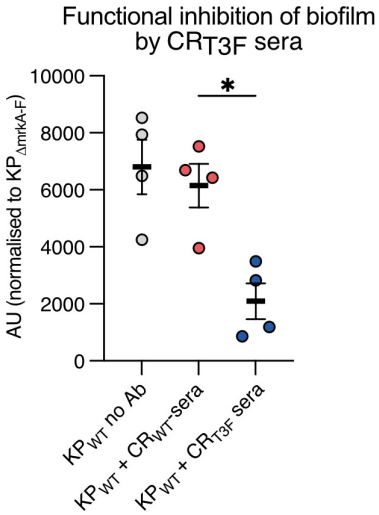

H.

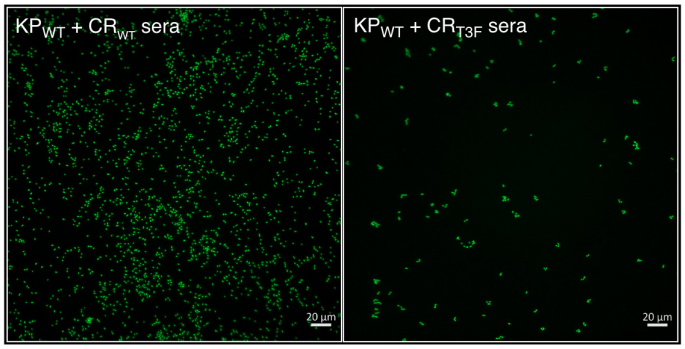

FIGURE 6.

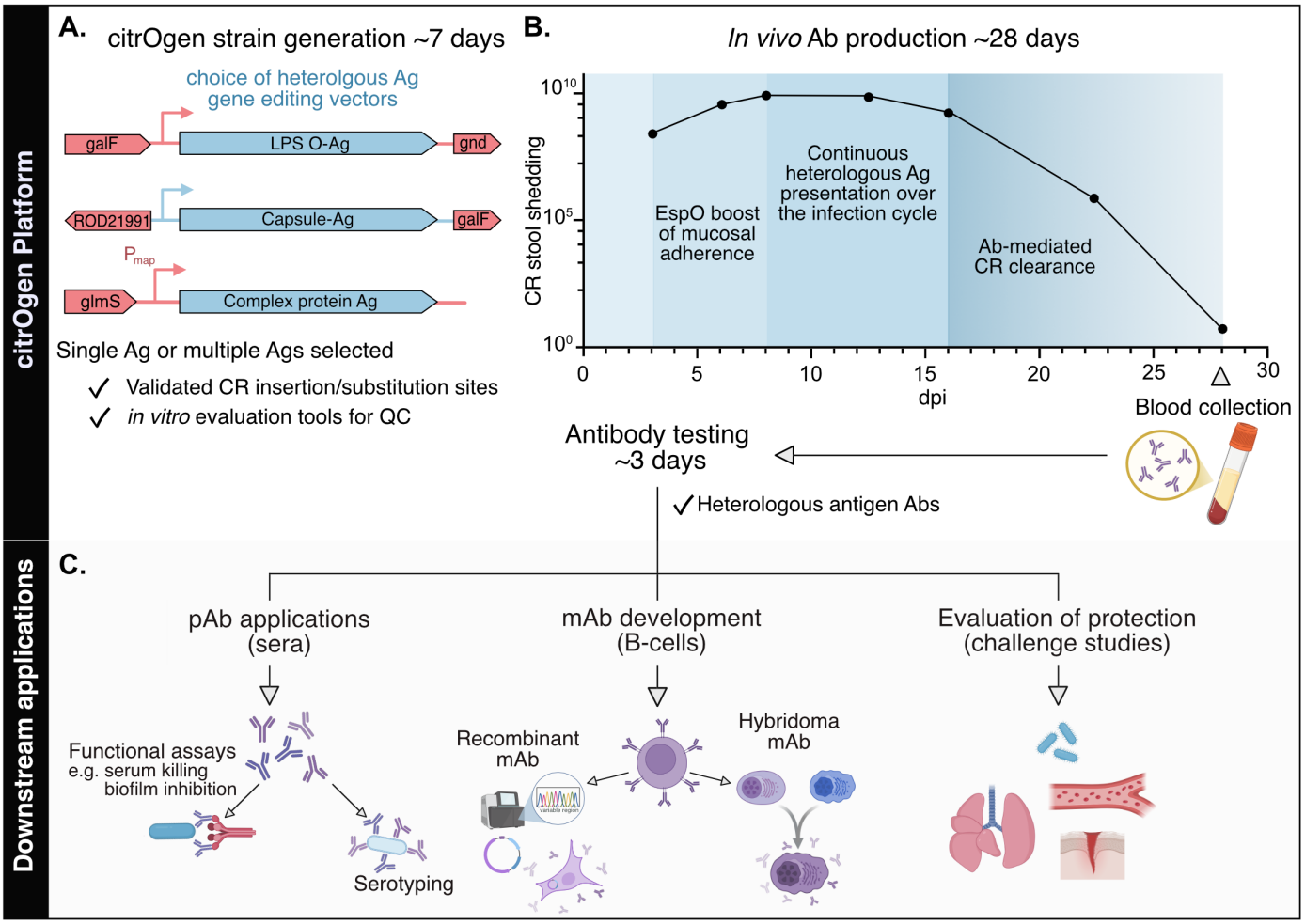
citrOgen Platform
A.
citrOgen strain generation ~7 days
choice of heterolgous Ag gene editing vectors
galF
LPS O-Ag
gnd
ROD21991
Capsule-Ag
galF
Pmap
glmS
Complex protein Ag
Single Ag or multiple Ags selected
✓ Validated CR insertion/substitution sites
✓ in vitro evaluation tools for QC
B.
In vivo Ab production ~28 days
CR stool shedding
10^10
10^5
10^0
EspO boost of mucosal adherence
Continuous heterologous Ag presentation over the infection cycle
Ab-mediated CR clearance
0
5
10
15
20
25
30
dpi
Blood collection
Antibody testing ~3 days
✓Heterologous antigen Abs
Downstream applications
C.
pAb applications (sera)
mAb development (B-cells)
Evaluation of protection (challenge studies)
Functional assays e.g. serum killing biofilm inhibition
Serotyping
Recombinant mAb
Hybridoma mAb

FIGURE 1.

A.

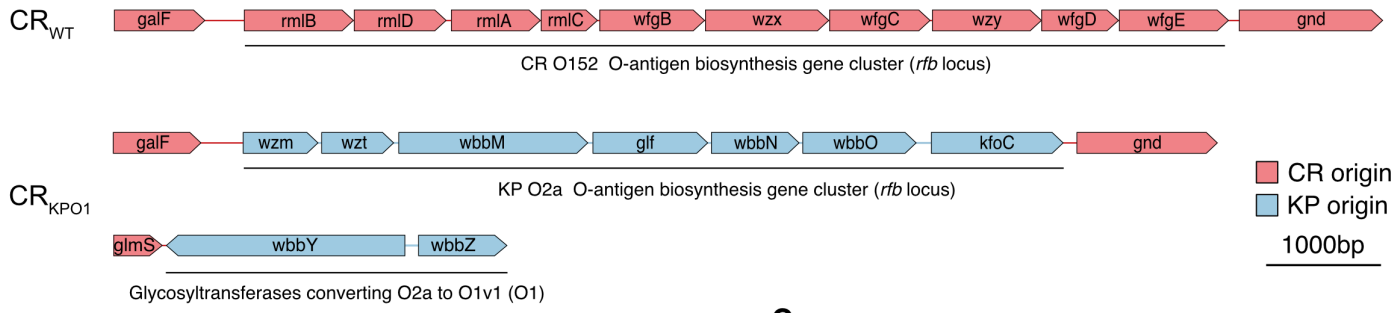

B.

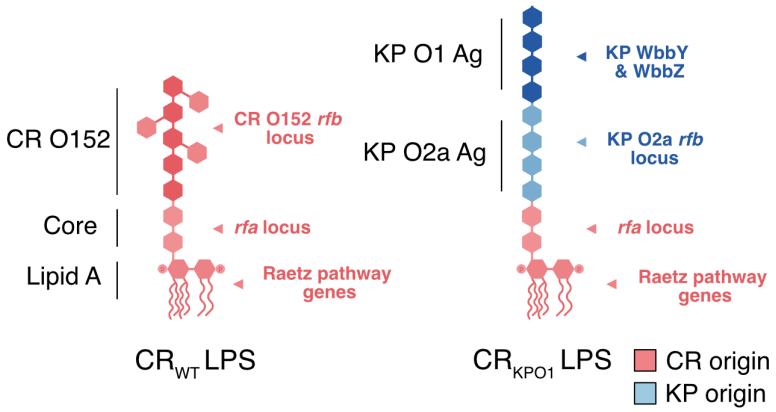

C.

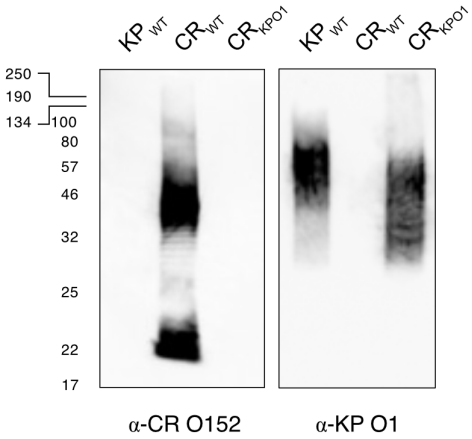

D.

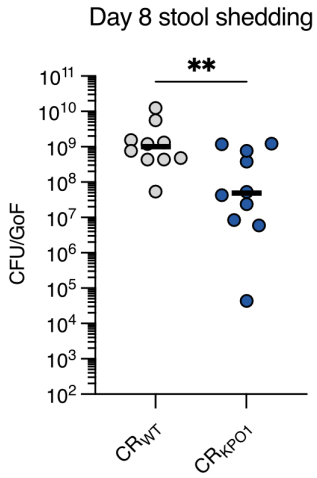

E.

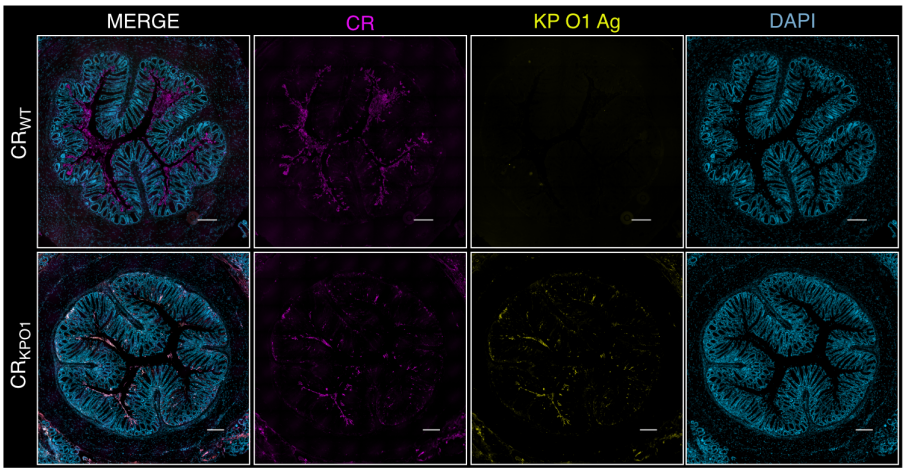

FIGURE 2.

A.

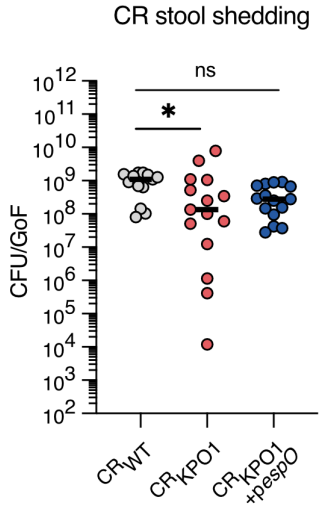

B.

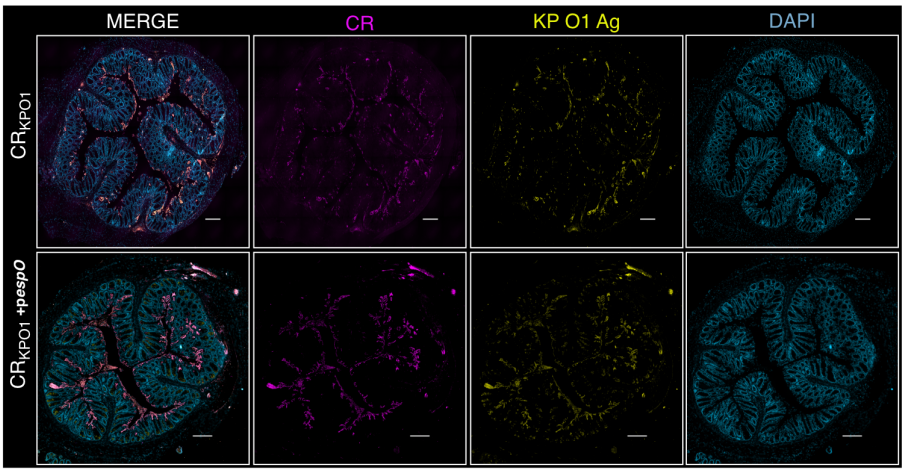

C.

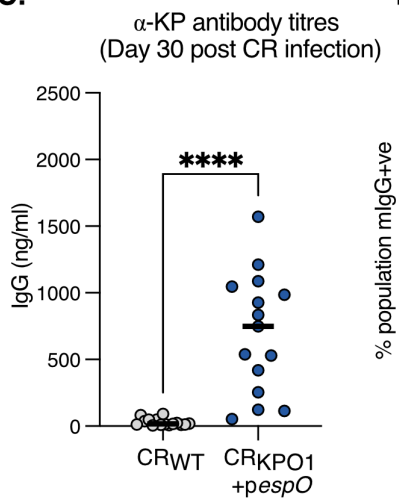

D.

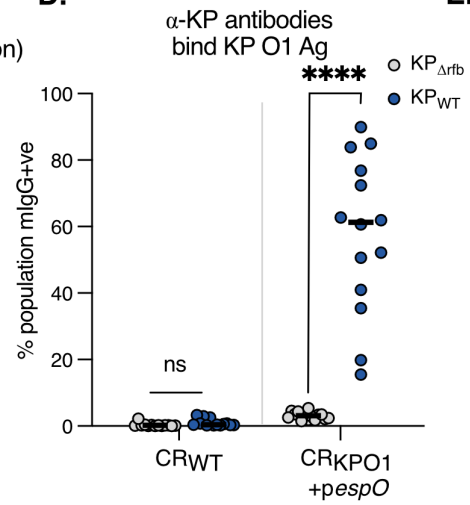

E.

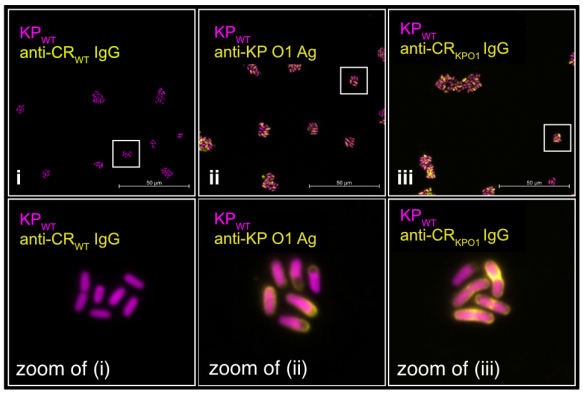

FIGURE 3.

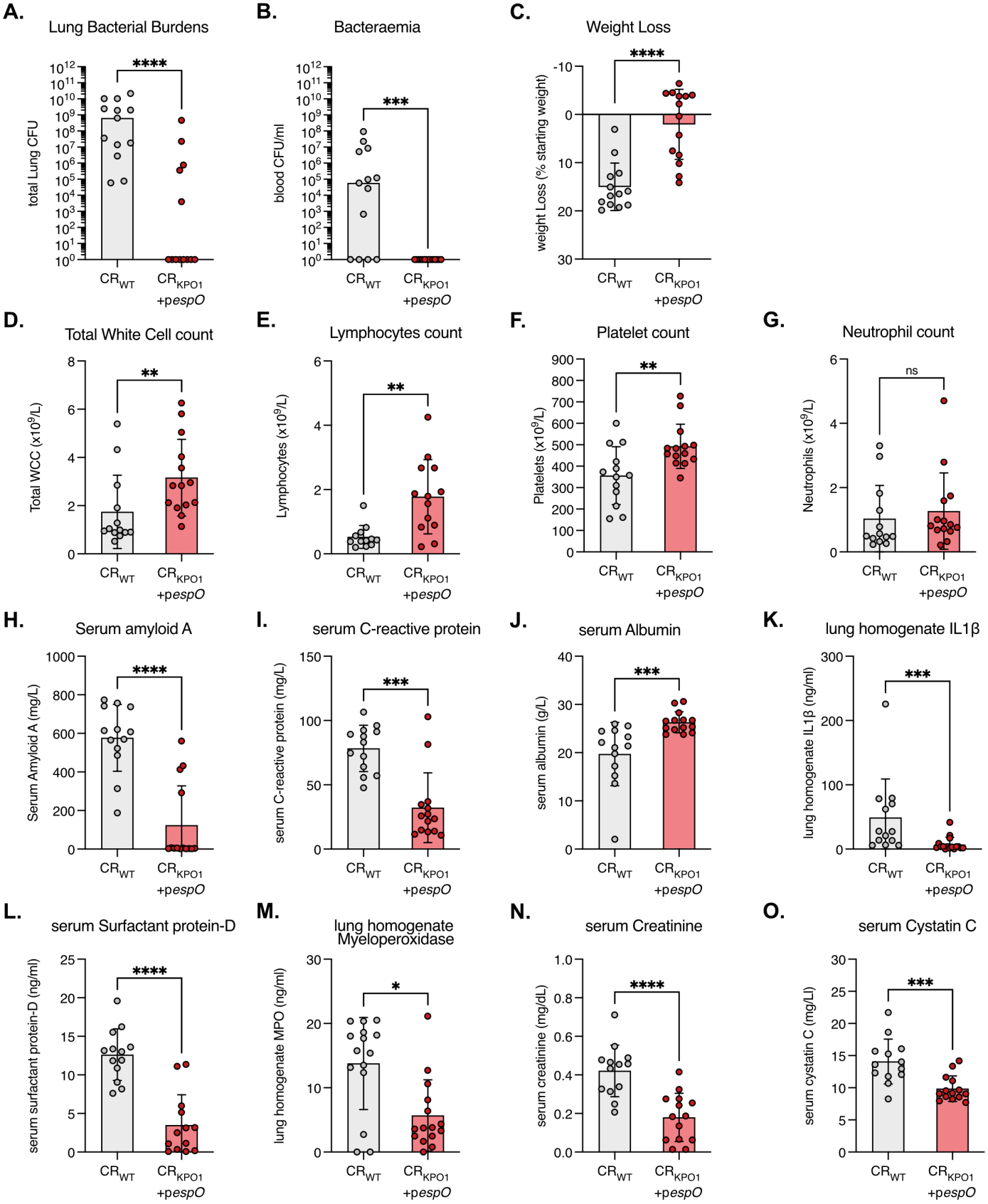
A.
Lung Bacterial Burdens
total Lung CFU
****
B.
Bacteraemia
blood CFU/ml
***
C.
Weight Loss
weight Loss (% starting weight)
****
D.
Total White Cell count
Total WCC (x10^9/L)
**
E.
Lymphocytes count
Lymphocytes (x10^9/L)
**
F.
Platelet count
Platelets (x10^9/L)
**
G.
Neutrophil count
Neutrophils (x10^9/L)
ns
H.
Serum amyloid A
Serum Amyloid A (mg/L)
****
I.
serum C-reactive protein
serum C-reactive protein (mg/L)
***
J.
serum Albumin
serum albumin (g/L)
***
K.
lung homogenate IL1β
lung homogenate IL1β (ng/ml)
***
L.
serum Surfactant protein-D
serum surfactant protein-D (ng/ml)
****
M.
lung homogenate Myeloperoxidase
lung homogenate MPO (ng/ml)
*
N.
serum Creatinine
serum creatinine (mg/dL)
****
O.
serum Cystatin C
serum cystatin C (mg/Ll)
***
CR_WT
CR_KPO1 +pespO

FIGURE 4.

A.

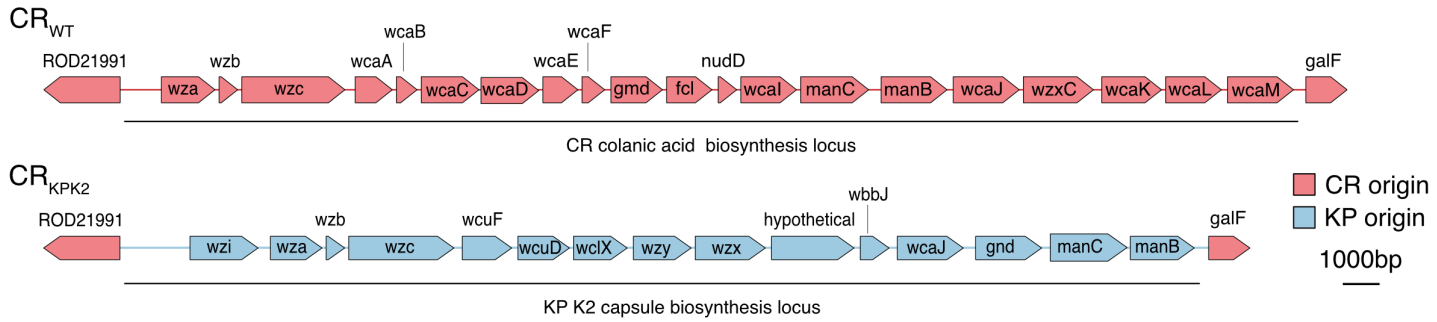

B.

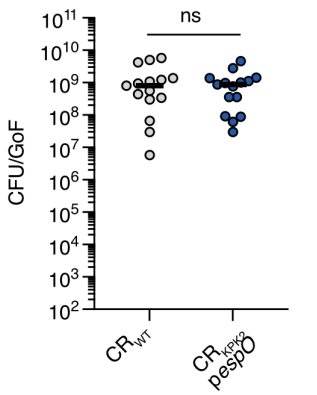

C.

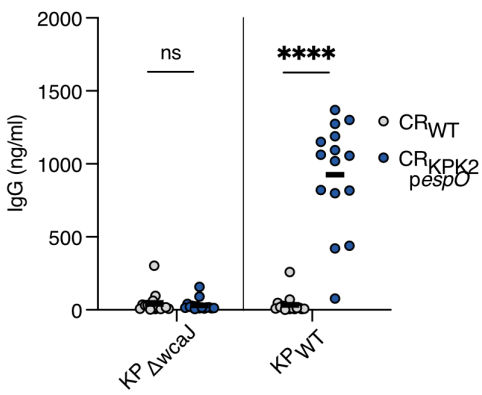

D.

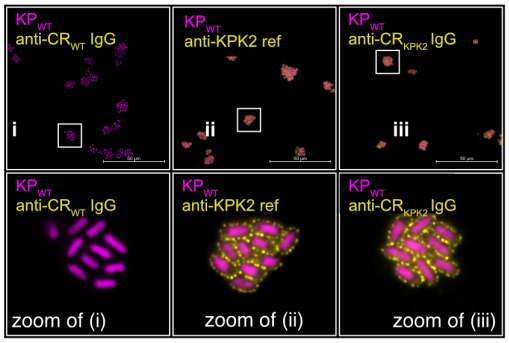

E.

KL25	KL31	KL38	KL38	KL148	KL30	KL62	KL17	KL3	KL25
KL23	KL10	KL3	KL17	KL142	KL60	KL62	KL113	KL42	KL63
KL2	KL14	KL28	KL24	KL28	KL105	KL151	KL102	KL30	KL52
KL19	KL30	KL119	KL110	KL3	KL154	KL146	KL27	KL15	KL125
KL51	KL64	KL2	KL52	KL57	KL5	KL3	KL25	KL51	KL57
KL21	KL107	KL15	KL113	KL58	KL51	KL10	KL2	KL30	KL1
KL43	KL30	KL64	KL61	KL27	KL9	KL46	KL36	KL116	KL62
KL2	KL35	KL20	KL28	KL13	KL61	KL2	KL51	KL112	KL14
KL102	KL62	KL39	KL30	KL46	KL15	KL14	KL65	KL54	KL107
KL122	KL46	KL15	KL2	KL2	KL128	KL62	KL107	KL64	KL107

KP$_{WT}$
KP$_{\Delta wcaJ}$

MFI signal key

2000
1000
500
250
125
62.5
31.3

F.

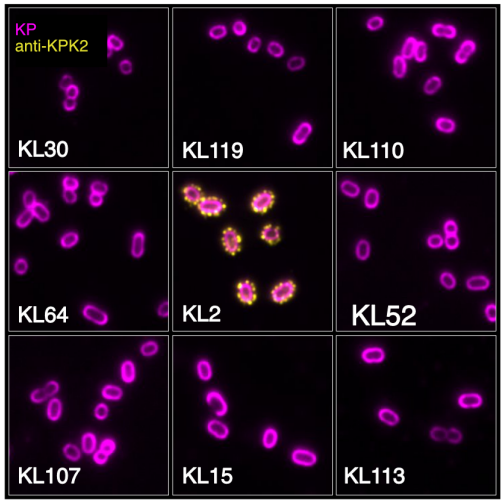

FIGURE 5.

A.

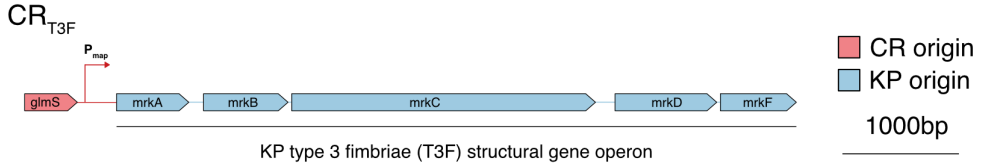

B.

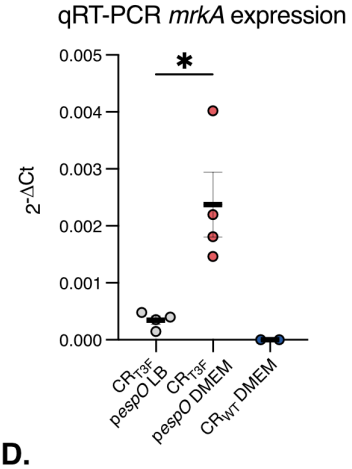

C.

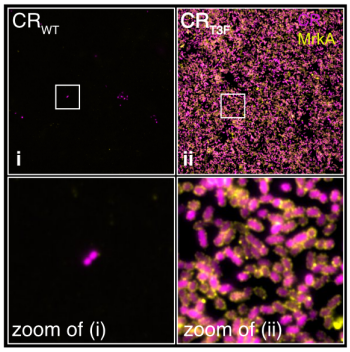

D.

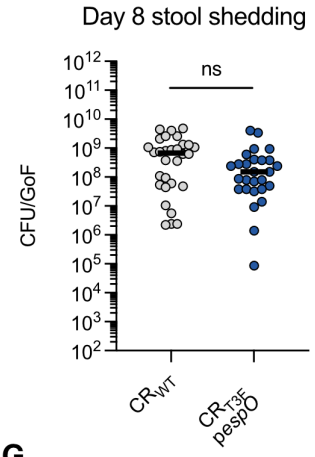

E.

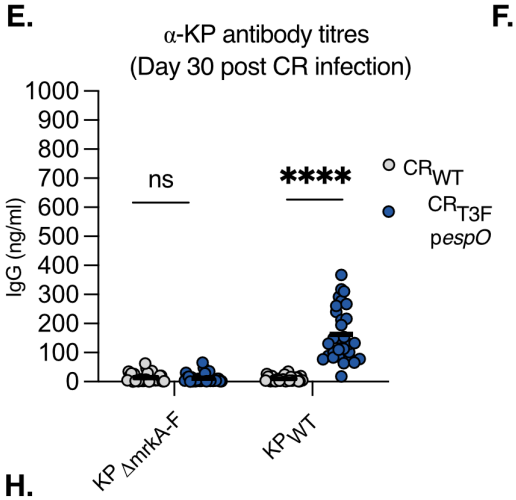

F.

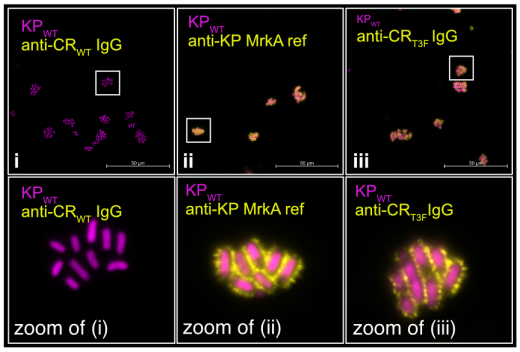

G.

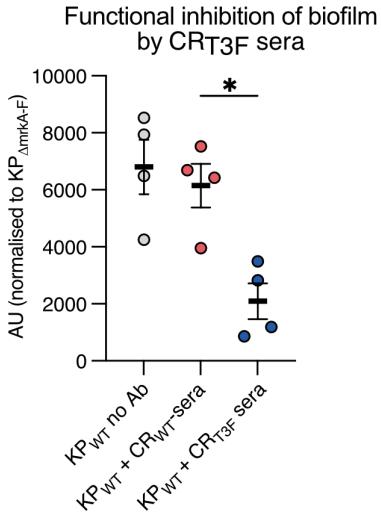

H.

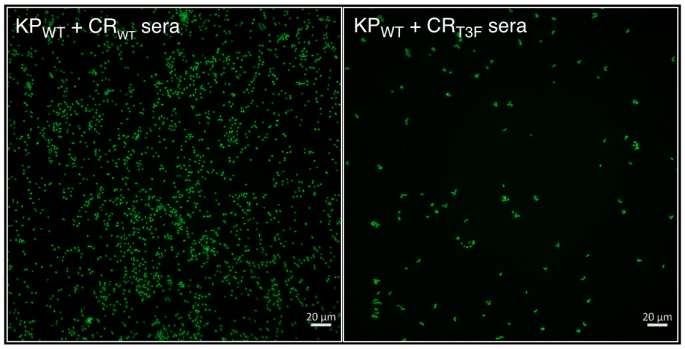

FIGURE 6.

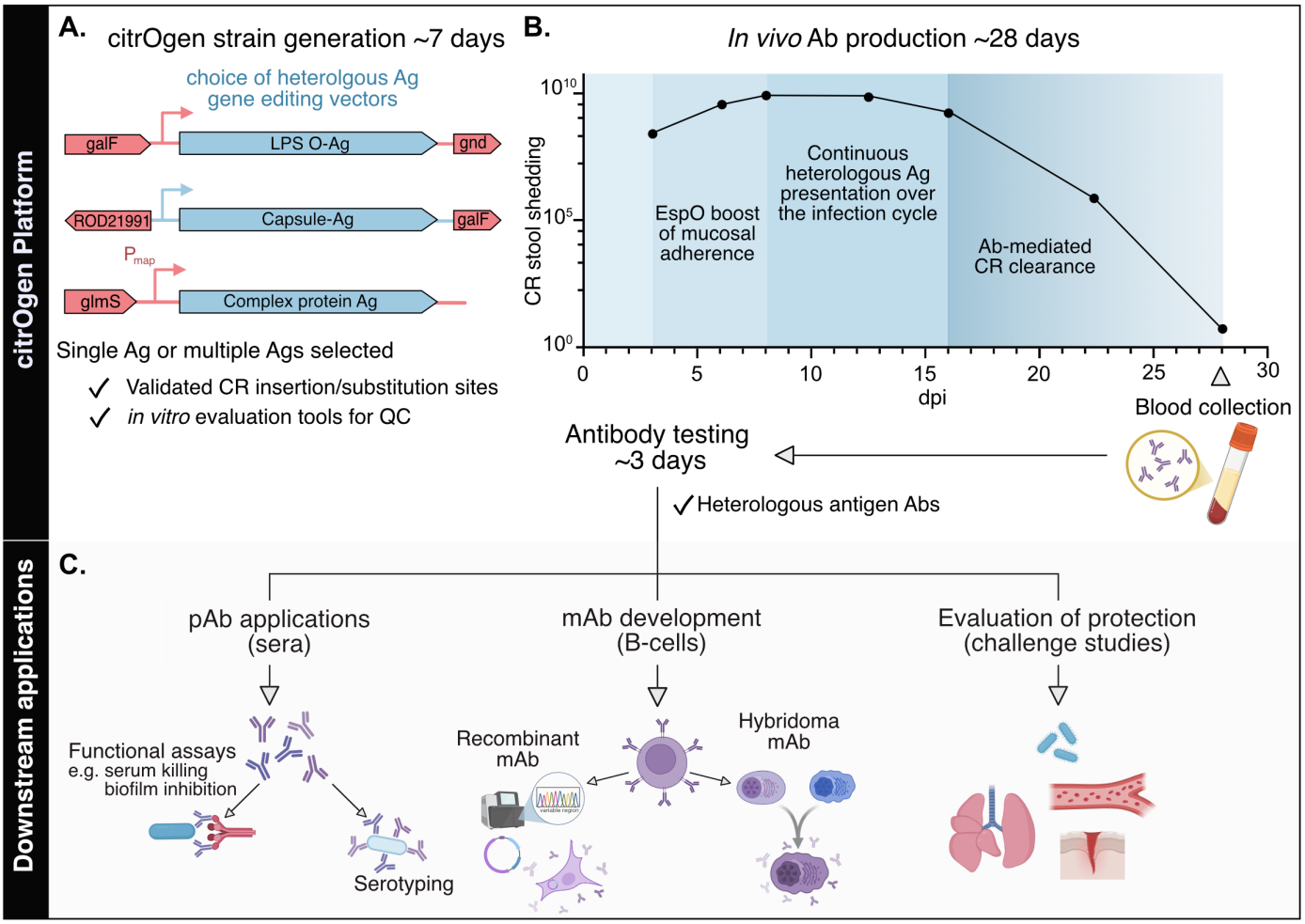
citrOgen Platform
A.
citrOgen strain generation ~7 days
choice of heterolgous Ag gene editing vectors
galF
LPS O-Ag
gnd
ROD21991
Capsule-Ag
galF
Pmap
glmS
Complex protein Ag
Single Ag or multiple Ags selected
✓ Validated CR insertion/substitution sites
✓ in vitro evaluation tools for QC
B.
In vivo Ab production ~28 days
CR stool shedding
10^10
10^5
10^0
EspO boost of mucosal adherence
Continuous heterologous Ag presentation over the infection cycle
Ab-mediated CR clearance
0
5
10
15
20
25
30
dpi
Blood collection
Antibody testing ~3 days
✓Heterologous antigen Abs
Downstream applications
C.
pAb applications (sera)
mAb development (B-cells)
Evaluation of protection (challenge studies)
Functional assays e.g. serum killing biofilm inhibition
Serotyping
Recombinant mAb
Hybridoma mAb